ELSEVIER

The thigh and leg of *Homo naledi*

Damiano Marchi [a, b, *], Christopher S. Walker [b, c, d], Pianpian Wei [b, e, f],
Trenton W. Holliday [b, g], Steven E. Churchill [b, d], Lee R. Berger [b], Jeremy M. DeSilva [b, h]

[a] Department of Biology, University of Pisa, Via Derna 1, Pisa 56126, Italy
[b] Evolutionary Studies Institute and Centre for Excellence in PalaeoSciences, University of the Witwatersrand, Private Bag 3, Wits 2050, South Africa
[c] Department of Molecular Biomedical Sciences, College of Veterinary Medicine, North Carolina State University, 1060 William Moore Drive, Raleigh, NC 27607, USA
[d] Department of Evolutionary Anthropology, Box 90383, Duke University, Durham, NC 27708, USA
[e] Key Laboratory of Vertebrate Evolution and Human Origins, Institute of Vertebrate Paleontology and Paleoanthropology, Chinese Academy of Sciences, Beijing 100044, China
[f] Department of Geoscience, University of Chinese Academy of Sciences, Beijing 100049, China
[g] Department of Anthropology, Tulane University, New Orleans, LA 70118, USA
[h] Department of Anthropology, Dartmouth College, Hanover, NH 03755, USA

ARTICLE INFO

ABSTRACT

This paper describes the 108 femoral, patellar, tibial, and fibular elements of a new species of *Homo* (*Homo naledi*) discovered in the Dinaledi chamber of the Rising Star cave system in South Africa. *Homo naledi* possesses a mosaic of primitive, derived, and unique traits functionally indicative of a bipedal hominin adapted for long distance walking and possibly running. Traits shared with australopiths include an anteroposteriorly compressed femoral neck, a mediolaterally compressed tibia, and a relatively circular fibular neck. Traits shared with *Homo* include a well-marked linea aspera, anteroposteriorly thick patellae, relatively long tibiae, and gracile fibulae with laterally oriented lateral malleoli. Unique features include the presence of two pillars on the superior aspect of the femoral neck and a tubercular distal insertion of the pes anserinus on the tibia. The mosaic morphology of the *H. naledi* thigh and leg appears most consistent with a species intermediate between *Australopithecus* spp. and *Homo erectus* and, accordingly, may offer insight into the nature of the earliest members of genus *Homo*. These fossils also expand the morphological diversity of the *Homo* lower limb, perhaps indicative of locomotor diversity in our genus.

© 2016 Elsevier Ltd. All rights reserved.

1. Introduction

The transition from *Australopithecus* to *Homo* probably involved changes to the postcranial skeleton (Bramble and Lieberman, 2004; Antón et al., 2014), but the limited number of postcranial remains assigned to early *Homo* has limited efforts to clarify the transition between the genera. There are isolated remains, such as KNM-ER 1472 (Leakey, 1973), KNM-ER 1481 (Kennedy, 1983), KNM-ER 5881 (Ward et al., 2015), and others (Wood and Leakey, 2011) that likely belong to *Homo*, however, given both the taxonomic diversity in early *Homo* (Leakey et al., 2012; Spoor et al., 2015; but see Van Arsdale and Wolpoff, 2012; Lordkipanidze et al., 2013) and

the spatial and temporal overlap between early *Homo* and the robust australopiths, attribution of isolated fossils to a species of early *Homo* remains speculative and controversial (e.g., Moyà-Solà et al., 2008). South African localities, in particular, have yielded very little postcranial material confidently attributed to *Homo* (but see McHenry, 1994; Susman et al., 2001).

The most complete specimens attributed to early *Homo*, which preserve both craniodental and lower limb remains, include OH 62 (Johanson et al., 1987; although the attribution of this specimen to *Homo* has been questioned; see Berger et al., 2010), KNM-ER 3735 (Leakey and Walker, 1985), and the *Homo erectus* fossils from Dmanisi, Georgia (Lordkipanidze et al., 2007). It has been suggested that the OH 62 femur is relatively short (Johanson et al., 1987; but see Haeusler and McHenry, 2004), with a long, anteroposteriorly compressed neck. Yet, both OH 62 and KNM-ER 3735 have well-developed femoral pilasters and levels of femoral diaphyseal

* Corresponding author.
  E-mail address: damiano.marchi@unipi.it (D. Marchi).

robusticity that are more human-like than those of australopiths, such as the *Australopithecus afarensis* partial skeleton A.L. 288-1 (Haeusler and McHenry, 2004, 2007). The diaphysis of the OH 62 femur, however, is not as mediolaterally expanded at the level below the lesser trochanter as is the A.L. 288-1 femur (Johanson et al., 1987). Limb proportions and general morphology of the Dmanisi lower limb are more human-like, although the Dmanisi remains also exhibit some primitive features in the foot and upper limb (Lordkipanidze et al., 2007; Pontzer et al., 2010). No other early *Homo* specimens are complete enough to provide an unambiguous attribution, making it difficult to characterize the lower limb of early members of our own genus.

Here, we describe the femora, patellae, tibiae, and fibulae of *Homo naledi* (Berger et al., 2015). Although the Dinaledi deposit is not yet dated, the overall cranial and postcranial morphology of *H. naledi* is most similar to Pleistocene fossils attributed to members of the genus *Homo* (Berger et al., 2015; Dembo et al., 2016).

2. Materials and methods

2.1. The Dinaledi and comparative sample

The thigh and leg remains of the Dinaledi assemblage consist of 108 femoral, patellar, tibial, and fibular elements (Table 1). Elements are defined as identifiable fossils (regardless of size or completeness) that do not clearly conjoin with any other known elements in the assemblage as it currently stands. The minimum number of individuals (MNI) and the maturity of the elements in the present sample were assessed using size, side, morphology, and epiphyseal fusion. Bone siding and anatomical overlap were the primary methods by which individuals in the postcranial assemblage were differentiated. Though the assemblage is remarkably homogenous morphologically, variation between bones of comparable size and from opposite sides was used in rare cases to distinguish unique individuals. State of epiphyseal fusion was used preferentially, wherever possible, in grouping elements into two broad developmental categories: mature (fused epiphyses) or immature (unfused epiphyses; no elements in the thigh and leg assemblage recovered to date have partially fused epiphyses). Size was used secondarily to estimate the maturity of fragmentary, isolated elements (not preserving epiphyses or metaphyses) and as a factor in differentiating individuals. Specimens that fell within or over the size range of elements determined to be mature by epiphyseal fusion were deemed mature. Elements markedly smaller than comparative mature specimens were designated immature. Maturity was not estimated for specimens of intermediate size. Overall, specimens sorted by size alone do not feature prominently in this work and are used primarily for classification purposes, whereas the most complete (typically preserving epiphyses or metaphyses) and thereby diagnostic elements of the assemblage are featured disproportionately in the present descriptions and analyses.

The femoral sample represents a minimum of eight mature and three immature individuals, while three mature individuals have been identified from the patellae. Seven mature and two immature individuals are known from the tibiae, and eight mature, two immature, and one individual of unknown developmental state are represented by the fibulae (Table 2). Descriptions of the most complete specimens are included in the main text. Descriptions of less anatomically informative fragments are presented in the Supplementary Online Material (SOM). The immature sample is pictured and described: it is largely morphologically consistent with the mature sample, but these specimens are excluded from diagnoses and analyses due to the potential for ontogenetic variation that cannot be fully evaluated at this time and is the subject of

Table 1
List of *Homo naledi* thigh and leg remains.

Catalog number	Element	Superoinferior preserved length (mm)
Femur		
U.W. 101-002	Right proximal femur	136.3
U.W. 101-003	Right femoral shaft	219.2
U.W. 101-012	Right femoral shaft	210.7
U.W. 101-014[a]	Femoral shaft	65.3
U.W. 101-018	Right proximal femur	97.5
U.W. 101-143	Right proximal femoral shaft	66.0
U.W. 101-215	Left distal femur	101.0
U.W. 101-268	Left femoral shaft	227.2
U.W. 101-271	Femoral head	35.8
U.W. 101-341	Femoral fragment	86.7
U.W. 101-398	Left proximal femur	144.1
U.W. 101-421	Left proximal femur	55.3
U.W. 101-545	Right distal femoral shaft	106.0
U.W. 101-857	Left distal femoral shaft	78.5
U.W. 101-898	Femoral condyle fragment	21.5
U.W. 101-938[a]	Right proximal femur	272.9
U.W. 101-1000[a]	Right proximal femur	95.2
U.W. 101-1098[a]	Right epiphyseal head	25.7
U.W. 101-1120[a]	Left distal femur	21.7
U.W. 101-1136	Right proximal femur	115.3
U.W. 101-1284	Right distal femoral shaft	158.4
U.W. 101-1300	Femoral head	35.2
U.W. 101-1391	Right proximal femur	137.2
U.W. 101-1434	Left proximal femur	83.0
U.W. 101-1475	Left proximal femur	99.3
U.W. 101-1482	Left femoral shaft fragment	121.9
U.W. 101-1523[a]	Right distal femoral shaft	84.3
U.W. 101-1555[a]	Femoral neck fragment with attached partial head	24.5
U.W. 101-1694[a]	Right distal femoral condyle	18.3
Patella		
U.W. 101-852	Right patella	24.9
U.W. 101-1404	Right patella	26.0
U.W. 101-1512	Partial patella	23.7
U.W. 101-1639	Right patella	23.0
Tibia		
U.W. 101-013	Distal tibial shaft	85.5
U.W. 101-017	Right proximal tibial shaft	57.0
U.W. 101-042[a]	Tibial shaft fragment	51.2
U.W. 101-072	Left distal tibial shaft	119.9
U.W. 101-085	Tibia shaft fragment	53.5
U.W. 101-136	Right proximal tibial shaft	92.5
U.W. 101-213	Right proximal tibial shaft	159.0
U.W. 101-237	Left proximal tibial shaft	59.6
U.W. 101-239	Proximal tibial shaft	109.8
U.W. 101-313	Left proximal tibial shaft	59.0
U.W. 101-402	Right distal tibial shaft	67.0
U.W. 101-420	Left distal tibia	82.7
U.W. 101-484	Right tibia	293.0
U.W. 101-498[a]	Left proximal tibial shaft	138.8
U.W. 101-500	Left proximal tibial shaft	144.4
U.W. 101-567	Tibia shaft fragment	58.7
U.W. 101-571	Right proximal tibial shaft	120.7
U.W. 101-586	Tibial shaft fragment	45.7
U.W. 101-711	Left distal tibia	48.3
U.W. 101-848	Right tibial shaft	124.9
U.W. 101-973	Left proximal tibial shaft	114.4
U.W. 101-996[a]	Right tibia	249.7
U.W. 101-1070[a]	Left tibia	278.0
U.W. 101-1210	Right distal tibial shaft	56.9
U.W. 101-1214	Right tibial midshaft	35.6
U.W. 101-1241	Left distal tibial shaft	63.5
U.W. 101-1262	Right distal tibia	36.5
U.W. 101-1288	Right distal tibial shaft	142.4
U.W. 101-1295	Tibial shaft fragment	42.1
U.W. 101-1416	Right distal tibia	42.2
U.W. 101-1518	Left distal tibia	29.8
Fibula		
U.W. 101-181	Distal fibular shaft	26.9
U.W. 101-416	Left proximal fibular shaft	28.7
U.W. 101-449	Proximal fibular shaft	25.9
U.W. 101-508	Right fibular midshaft	47.9

Table 1 (*continued*)

Catalog number	Element	Superoinferior preserved length (mm)
U.W. 101-580	Left distal fibular shaft	59.1
U.W. 101-675	Proximal fibular shaft	21.8
U.W. 101-702	Left proximal fibular shaft	65.5
U.W. 101-719	Left proximal fibular shaft	57.5
U.W. 101-722	Proximal fibular shaft	23.3
U.W. 101-737	Right distal fibular shaft	38.0
U.W. 101-778	Distal fibular shaft	17.9
U.W. 101-782	Distal fibular shaft	38.6
U.W. 101-806	Fibula shaft fragment	25.5
U.W. 101-813	Fibula shaft fragment	26.7
U.W. 101-817[a]	Proximal left fibula	34.3
U.W. 101-876	Proximal fibular shaft	20.4
U.W. 101-892	Distal fibular shaft	45.9
U.W. 101-902	Left proximal fibular shaft	61.9
U.W. 101-925	Right proximal fibular shaft	89.4
U.W. 101-968	Right distal fibular shaft	115.6
U.W. 101-987	Proximal fibular shaft	22.6
U.W. 101-1037	Proximal left fibular shaft	238.0
U.W. 101-1045[a]	Left fibula	207.5
U.W. 101-1046	Left distal fibular shaft	31.0
U.W. 101-1066	Fibular midshaft	84.9
U.W. 101-1071	Distal fibular shaft	30.2
U.W. 101-1094	Fibula shaft fragment	24.4
U.W. 101-1113	Right proximal fibular shaft	34.7
U.W. 101-1114	Distal fibular shaft	32.9
U.W. 101-1115	Fibular midshaft	35.3
U.W. 101-1122	Fibula shaft fragment	32.5
U.W. 101-1138	Proximal fibular shaft	21.5
U.W. 101-1143	Right fibular shaft	54.7
U.W. 101-1231	Distal fibular shaft	22.0
U.W. 101-1254	Right proximal fibular shaft	112.5
U.W. 101-1259	Fibula shaft fragment	21.0
U.W. 101-1260	Left proximal fibular shaft	59.0
U.W. 101-1313	Proximal fibular shaft	48.3
U.W. 101-1436	Fibular midshaft	38.7
U.W. 101-1437	Right distal fibula	21.4
U.W. 101-1451	Left proximal fibular shaft	36.1
U.W. 101-1520	Fibula shaft fragment	26.0
U.W. 101-1679	Right proximal fibular shaft	27.6
U.W. 101-1701	Left distal fibula	23.6

[a] Immature status based on the presence of unfused epiphysis or size (see Methods)

Table 2
Summary of the Dinaledi Chamber thigh and leg remains. Minimum number of elements (MNE) and minimum number of individuals (MNI) by each element.

Element	MNE			MNI		
	Mature	Immature	Total	Mature	Immature	Total
Femora	21	8	29	8	3	11
Patellae	4		4	3		3
Tibiae	27	4	31	7	2	9
Fibulae	42	2	44	9	2	11
	Total MNE		108	Total MNI		11

ongoing study. The comparative samples used in the analyses are listed in SOM Tables S1 and S2. In summary, it includes the following groups: extant species *Homo sapiens*, chimpanzee (*Pan troglodytes*) and gorilla (*Gorilla gorilla*), and fossil species *Orrorin tugenensis*, *Australopithecus* (which includes *A. afarensis*, *Australopithecus africanus*, *Australopithecus sediba*, *Australopithecus robustus,* and *Australopithecus boisei*), hominin indet. (see SOM Table S1 for the specimens included), Early *Homo* (see SOM Table S1 for the specimens included) and *H. erectus*.

2.2. Femur methods

Measurements taken on the proximal femur include the maximum superoinferior (SI) diameter of the femoral head, the minimum SI diameter of the neck (taken such that the measurement was orthogonal to the long axis of the bone), and the anteroposterior (AP) diameter of the neck (taken orthogonal to the SI diameter of the neck). These measures followed measurement numbers 1—3 in McHenry and Corruccini (1978) and repeated in other hominin femoral studies (e.g., Reed et al., 1993). Because no femora preserved both the head and the greater trochanter, biomechanical neck length was not measured. Instead, the neck was measured as the maximum length along the main axis from the lateralmost edge of the femoral head to the intertrochanteric crest (measurement number 7 in McHenry and Corruccini [1978]). No *H. naledi* femora are complete, so femoral anteversion could not be measured using the traditional method (Kingsley and Olmsted, 1948). Instead, femoral neck anteversion was quantified as the angle formed by the longitudinal axes of the neck and the proximal shaft, with the shaft positioned so that the linea aspera distal to the point of convergence between the spiral line and the gluteal line is the most posterior part of the bone (Fig. 1). Digital photos were taken with the lens in line with the bone and perpendicular to the superior view of the femur (Fig. 1b). The photograph obtained is shown in Figure 1c. ImageJ (http://rsb.info.nih.gov/ij/) was used to measure anteversion angle on the digital photos, which were measured as the angles between the longitudinal axis of the neck and the sagittal plane (Fig. 1c). Angles greater than 90° indicate femoral neck anteversion. A typical modern human angle is lower than 90° (Fig. 1c).

Femoral neck external outlines in sagittal view (Fig. 2) were taken at the neck—shaft junction on three-dimensional (3D) digital scan reconstructions. Three-dimensional digital scans were captured using a 3D HD Next Engine Scanner in wide mode: 380 μm accuracy and 6 points per mm. The subtrochanteric dimensions were measured as the maximum mediolateral (ML) diameter of the shaft below the lesser trochanter and the AP diameter of the bone perpendicular to the ML diameter as described in McHenry and Corrucini (1978; measurements 4 and 5) and Gilbert (2008). Ratios were used to characterize the shape of the femoral neck (AP/SI*100) and the platymeric index (AP/ML*100). Relative neck length was assessed by dividing the neck length by the square root of the product of the ML and AP subtrochanteric dimensions. To justify the use of ratios, reduced major axis (RMA) regressions were used to demonstrate that the 95% C.I. of the slope of the line characterizing the scaling relationship between the two variables used in the ratio included 1.0.

Medical computed tomography (CT) scanning of three mature femoral diaphyses (U.W. 101-003, UW. 101-012, and U.W. 101-268) was performed at Johannesburg Hospital (Johannesburg, South Africa) on a Philips Brilliance 16P medical CT scanner (Philips Healthcare, Andover, MA); pixel dimensions 0.98 × 0.98 mm. Following data acquisition, image stacks were segmented to produce isosurfaces using Avizo 8 software (Visualization Sciences Group, Mérignac, France). In order to create diaphyseal cross-sections, the medullary spaces must be identified and matrix needs to be subtracted by manual segmentation. Because of the low resolution of the images, it was not possible to accurately isolate the cortical shell of specimens U.W. 101-003 and U.W. 101-012. U.W. 101-268 did not present matrix in the medullary cavity, thus allowing segmentation. Due to the fragmentary nature of U.W. 101-268, midshaft level was first estimated on the more complete U.W. 101-003 and then estimated on U.W. 101-268 by positioning the two bones parallel to each other. Given that the two femoral diaphysis roughly represent the same portion of the femur (see descriptions below) this approach is justified by evidence for low variability in cross-sectional geometry around the midshaft in modern humans (Sládek et al., 2010). Cross-sectional images obtained with Avizo 8 were imported into Image J and analyzed using MomentMacro 1.3 (http://www.hopkinsmedicine.org/FAE/mmacro.html).
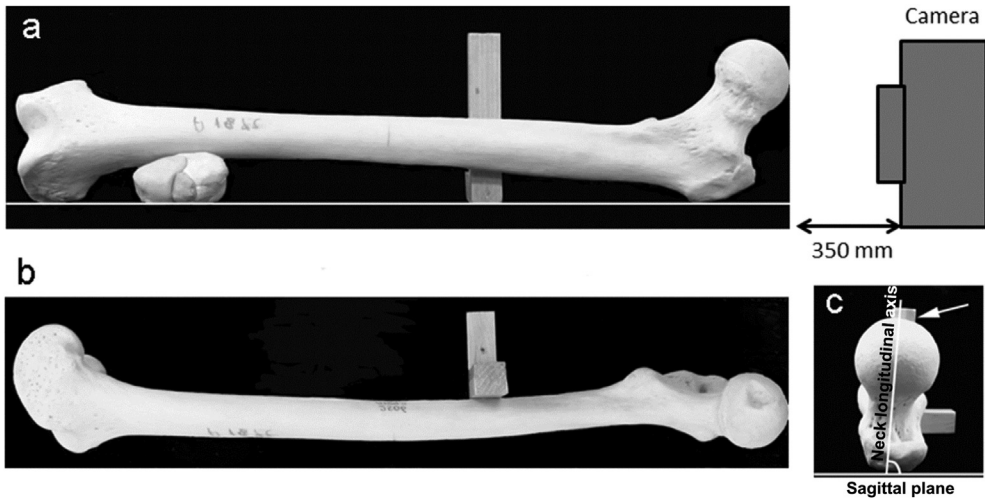
Figure 1. Method used to quantify femoral neck anteversion relative to the proximal shaft on a left human femur. (a) Anterior view, (b) medial view, (c) cranial view (anterior to the left and posterior to the right). White arrows indicate the L-square used to position the linea aspera. See text for explanation.
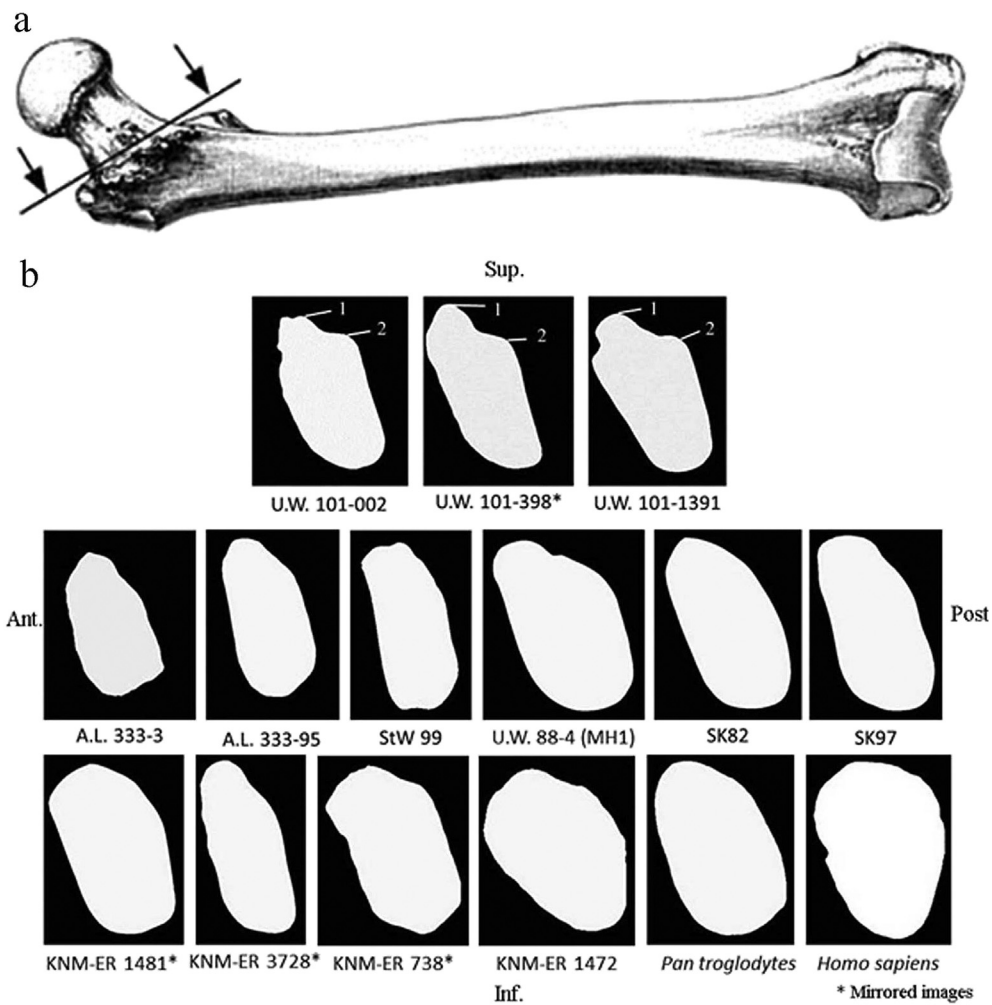

Figure 2. Femoral neck sagittal outlines. (a) Black arrows indicate the neck/shaft junction where sections of the femoral neck were taken; (b) external outlines in sagittal view at the neck–shaft junction are shown for *Homo naledi* (U.W. 101-002, U.W. 101-398, and U.W. 101-1391) and compared to other fossil hominins, chimpanzees, and modern humans. Note the presence of two pillars on the superior aspect of the femoral neck of *H. naledi*, one superoanterior (1) and the other inferoposterior (2). The pit between the two may signify a more medially encroaching lateral attachment for mm. obturator internus and gemelli in *H. naledi*. Sup. = superior, Inf. = inferior, Ant. = anterior, Post = posterior.

A linear discriminant function analysis (DFA) was performed to classify the Dinaledi femora relative to known hominin femora. Five measurements of the proximal femur described earlier were used in DFA: neck SI, neck AP, subtrochanteric AP, subtrochanteric ML, and neck length. The five variables were size-adjusted by dividing each variable by the geometric mean of the five proximal femoral measurements (Mosimann, 1970; Richmond and Jungers, 2008). In the first DFA, the Dinaledi femora were entered as unknowns alongside *H. sapiens*, *Australopithecus*, fossil *Homo*, and hominin indet. This last grouping consisted of five femora (KNM-ER 738, KNM-ER 815, KNM-ER 1463, KNM-ER 3728, and KNM-ER 5880) that could either be from early *Homo* or robust *Australopithecus*. Because of this taxonomic uncertainty, a second DFA was performed without these hominin indet. specimens. The DFA was performed using IBM SPSS Statistics Version 20.

2.3. Patella methods

Patella measurements included the maximum SI diameter of the bone (M1), the maximum ML breadth (M2), and the maximum AP thickness (M3) following Martin and Saller (1957). The relative AP thickness of the patella was assessed as: (AP/ML*100).

2.4. Tibia methods

The tibial nutrient foramen and midshaft dimensions were measured as the maximum AP diameter of the shaft at the nutrient foramen and midshaft, respectively, and the ML diameter of the bone perpendicular to the AP diameters. Distal tibia measurements included the maximum ML thickness of the medial malleolus, the maximum ML diameter of the anterior and posterior rims of the talar articular surface, and the ML diameter of the midpoint of the talar facet following the methods described in DeSilva (2008).

Tibia length (intended as total length, M1 [Martin and Saller, 1957]) obtained from the only nearly complete mature specimen (U.W. 101-484) was estimated using two methods: 1) a comparative measure obtained from a human tibia (Khoe-san) at the University of the Witwatersrand fossil lab of approximately the same size as U.W. 101-484 (Fig. 3; yielding an estimated length of 325 mm), and 2) a measure derived from Wright and Vásquez's (2003) regression formulae obtained from a Guatemalan population. Forensic-based regressions using articular dimensions to estimate bone length (Chibba and Bidmos, 2007) are not applicable given that U.W. 101-484 lacks complete epiphyses, however, regressions based on diaphyseal dimensions can be applied (Steele and McKern, 1969; Jacobs, 1992; Wright and Vásquez, 2003). We are aware that these formulae are population specific (Wright and Vásquez, 2003) and can vary with muscular activity patterns and intensity (Jacobs, 1992). Nevertheless, the formulae developed for the Guatemalan population can be tentatively used, given the diminutive stature and relatively gracile skeletons of this population, similar to that seen in *H. naledi*. U.W. 101-484 includes the most proximal point of the tibial tuberosity to the proximal margin of the tibiotalar articular surface (called T1–T6 in Wright and Vásquez, 2003), and is related to total tibial length by the equation:

$$T1 - T6 = 8.847 + 0.873 \times \text{tibia length} \ (R^2 = 0.965; N = 89; SE = 5.92).$$

U.W. 101-484 does not preserve enough of the articular surface distally (or any of the proximal articular surface) to compare the length to the weight bearing joints of this individual. Thus, to assess the relative length of the tibia, we performed a bootstrapping analysis that produced normal distributions for tibial length

Figure 3. The tibia and fibula from a Khoe-San skeleton is compared with the fragmentary U.W. 101-484 tibia to help estimate *Homo naledi* tibial length. The proximal break in the U.W. 101-484 tibia is just proximal to the tibial tubercle and it is at the same level of the tibial tubercle of the Khoe-San tibia. Also note the gracility (compared to tibial length) of the *H. naledi* tibia compared to the modern human.

compared to the femoral head diameter in humans and great apes. The femoral head SI measurement for U.W. 101-484 along with the diameter of two mature femoral heads (U.W. 101-271 [35.8 mm] and U.W. 101-1300 [35.2 mm]) were used in this analysis. Tibial lengths from humans ($n = 122$), lowland gorillas ($n = 16$), chimpanzees ($n = 24$), and orangutans ($n = 12$) were compared with femoral head diameters from humans ($n = 308$), lowland gorillas ($n = 112$), chimpanzees ($n = 125$), and orangutans ($n = 23$; see SOM Table S3) using the resampling macro in Microsoft Excel (Resampling Stats Excel Add-in Version 4). In humans, a single tibial length was randomly selected and divided by the average of two randomly sampled femoral head diameters. This was repeated 5000 times, and then repeated for the great apes using an exact randomization approach given the smaller sample sizes. Normal distributions of tibial length:femoral head diameter resulted and we assessed the likelihood of sampling the ratio found in the Dinaledi sample to that constructed for humans and great apes.

2.5. Fibula methods

Fibula measurements included AP (M4c) and ML (M4b) neck diameter, where the neck is the region of the proximal fibular diaphysis of lowest circumference, and midshaft AP [(M3(2)] and ML [(M3(1)] diameters following Martin and Saller (1957). The linear measurements were used to compute the neck robusticity index and the midshaft robusticity index of the fibula: (ML/AP*100).

U.W. 101-1037 is the most complete fibula of the Dinaledi assemblage and is preserved from the level of the neck to just inferior to the most proximal part of the insertion of the interosseous ligament. Unfortunately, no data are available in the literature to estimate fibula length from fragmentary bones. Accordingly, we developed a new length estimation method using two landmarks on the fibular diaphysis: the proximal neck and the most proximal part of the subcutaneous triangular surface (STS). We measured neck-STS distance (intended as the distance, parallel to the longitudinal axis of the fibula, between the neck and the most proximal part of the STS) and fibular total length (M1, Martin and Saller, 1957) from a South African sample housed at the Dart Collection, University of the Witwatersrand. The sample includes 31 non-pathological adult individuals. A regression formula was obtained to estimate fibular total length:

Fibula length (mm) = 62.761 + 1.282 × neck-STS (R^2 = 0.735; N = 31; SEE = 9.7).

The angle between the fibulotalar surface area and STS was measured following Stern and Susman (1983). The fibulotalar articular surface has been divided into two functional surfaces: the proximal portion, which articulates with the vertical part of the lateral articular surface of the talus, and the distal portion that articulates with the flaring part of the lateral articular surface of the talus (Marchi, 2015). The AP and SI diameters of the proximal and distal portions of the fibulotalar articulation were measured and used to calculate the areas of the two articular surfaces (Marchi, 2015).

3. Descriptions of Dinaledi thigh and leg remains

3.1. Femur

Dimensions for the *H. naledi* femur sample are listed in Table 3. Femur specimens are depicted in Figures 4 – 11 (3D surface scans available at www.morphosource.org).

U.W. 101-002 (Fig. 4a) is a mature right proximal femur preserved from the proximal end of the eroded head to a clean break in the shaft. Posteriorly, there is a ring of cortex around the damaged head that flares gradually and is fenestrated with vascular foramina demarcating the head–neck junction. The neck is well preserved posteriorly, but has some damage anteriorly. It is AP compressed. The femoral head and neck are anteverted relative to the long axis of the shaft. There is a palpable obturator externus groove across the posterior neck. Superiorly, along the neck, there are two ML oriented pillars of bone (see Fig. 5 for examples). One is more inferior and posterior, the other is more superior and anterior. These contribute to torsion of the head and neck relative to the long axis of the shaft. Anteriorly, the neck is smooth without any evidence of an intertrochanteric line. Anterolaterally, there is a palpable depression for m. vastus lateralis. The underlying trabecular bone is all that remains of the badly damaged greater trochanter, which is 25.3 mm AP and 23.2 mm ML. At the superior junction of the neck and the greater trochanter, there is a part of the trochanteric fossa preserved in which there are several vascular foramina. In anterior view, the inferior aspect of the greater trochanter flares laterally. The lesser trochanter is badly eroded, though the overall dimensions are about 14.3 mm SI and 13.6 mm ML. It is positioned posteriorly and cannot be seen in anterior view, likely because of erosion. The center of the lesser trochanter is 28.8 mm from the inferolateral edge of the femoral head. Just inferior to the lesser trochanter, the shaft is platymeric. Descending straight from the edge of the greater trochanter posterolaterally is a well-developed third trochanter. Lateral and inferior to the gluteal line is a concave depression—the hypotrochanteric fossa. Lateral to that is a thickening of the cortex that begins anterolaterally and spirals inferiorly to merge with the gluteal line just inferior to the hypotrochanteric fossa. The central part of the posterior shaft is abraded and the pectineal and spiral lines are barely detectable. Inferiorly, the lines merge into a well-developed linea aspera. Anteriorly, the shaft is convex, posteriorly it is relatively flat. The shaft at the point of break is circular: 20.0 mm ML and 20.6 mm AP. Here, the medial cortex is thicker (6.7 mm) than the lateral cortex (6.3 mm).

U.W. 101-003 (Fig. 6) is a large right femoral shaft, from a break just below the lesser trochanter to a break in the shaft that precedes the supracondylar split of the linea aspera. It is platymeric near the subtrochanteric region. The ML narrowest part of the shaft appears to be quite distal, near the break. Proximally and posterolaterally there is a rugose gluteal line lateral to which is the base of the hypotrochanteric fossa. Just medial to the gluteal line is a pectineal line that merges with the gluteal line 23.5 mm inferior to the break in the proximal shaft. The spiral line can be traced proximomedially down the shaft and merges with the other two muscle markings 58.2 mm down the shaft to form a linea aspera that runs the length of the preserved bone. Distolaterally, the shaft has a weak concavity, just lateral to the linea aspera. Anteriorly, the shaft is quite flat proximally and becomes more rounded distally. Proximally and medially there is a depression that runs to approximately midshaft between the convex anterior and medial aspects of the bone, which is likely a consequence of the torsion of the proximal diaphysis. In medial and lateral view, the bone is AP curved. The dimensions at the point of the distal break are 25.3 mm AP and 21.7 mm ML.

U.W. 101-012 (Fig. 6) is a right femoral shaft. It is AP broad throughout, meaning that its proximal break is likely more distally positioned than the subtrochanteric region, which is platymeric in the Dinaledi femora. A break in the bone distally has internal trabeculae indicating proximity to the knee region. Proximally, the shaft is 21.8 mm AP and 19.9 mm ML. Here, the medial cortex is thicker (6.7 mm) than the lateral cortex (5.7 mm). At the distal break, it is 25.1 mm AP and 20.1 mm ML. In medial and lateral views, there is some AP curvature to the shaft. In anterior view, the shaft is somewhat bowed ML (convex medially).

U.W. 101-018 (Figs. 4b, 7) is a mature right proximal femur preserving the neck, greater trochanter, and proximal shaft. The head is not preserved and the neck is too badly damaged to measure dimensions. The break in the neck reveals internal trabeculae and asymmetrical cortical bone at the neck/shaft junction, measuring (approximately) 1.5 mm superiorly and 9.5 mm inferiorly in thickness. There is erosion around the perimeters of the lesser and greater trochanters revealing trabecular bone. There is some abrasion along the shaft, but the cortex is preserved well enough to detect muscle markings. Posteriorly, the neck is smooth without an obvious obturator externus groove. Superiorly, the neck is bordered by a prominent bar of bone lateral to which is a well-developed trochanteric fossa. Anteriorly, the neck is damaged and exposed trabeculae extend from the greater trochanter to the femoral neck. There is a palpable depression for m. vastus lateralis. Just medial to the depression is the inferior extent of the intertrochanteric line that continues medial and inferior to the lesser

ARTICLE IN PRESS

Table 3
Comparative femur dimensions.[a]

Specimen/Species	Head diameter (mm)	Neck SI (mm)	Neck AP (mm)	Neck shape (AP/SI) × 100	Neck–shaft angle (degrees)	Neck length[b] (mm)	Neck length/subtrochanteric dimensions[c]	Subtroch. AP (mm)	Subtroch. ML (mm)	Platymeric index	Femoral anteversion (degrees)
U.W. 101-002	–	22.6	15.0	66.4	115.7	30.0	1.44	18.5	23.6	78.4	118.9
U.W. 101-003	–	–	–	–	–	–	–	21.6	31.4	68.8	–
U.W. 101-018	–	–	–	–	–	–	–	18.1	23.8	76.1	–
U.W. 101-143	–	–	–	–	–	–	–	17.6	20.2	87.1	–
U.W. 101-268	–	–	–	–	–	–	–	21.1	26.3	80.2	–
U.W. 101-271	35.8		–	–	–	–	–	–	–	–	–
U.W. 101-398	–	22.9	16.1	70.3	118.2	34.3	1.60	19.1	24.0	79.6	114.5
U.W. 101-421	33.5[e]	25.8	16.9	65.5	–	32.8	–	–	–	–	–
U.W. 101-1136	–	–	–	–	–	–	–	16.9	25.5	66.3	–
U.W. 101-938[d]	25.9	22.0	16.0	72.7	112.0	28.1	1.59	15.9	19.6	81.1	–
U.W. 101-1000[d]	25.7	20.9	16.7	79.9	117.6	–	–	16.7	19.9	–	–
U.W. 101-1300	35.2	–	–	–	–	–	–	–	–	–	–
U.W. 101-1391	–	21.7	17.5	80.7	118.0	27.4	1.29	18.8	23.9	78.7	108.6
U.W. 101-1434	–	–	–	–	–	–	–	15.4	19.1	80.6	–
U.W. 101-1475	–	–	–	–	–	–	–	18.8	29.0	64.8	118.9
U.W. 101-1482	–	–	–	–	–	–	–	20.7	28.9	71.6	–
U.W. 101-1555[d]	24.3[e]	–	14.3	–	–	–	–	–	–	–	–
Homo naledi[f]	35.5 ± 0.4	23.3 ± 1.8	16.4 ± 1.1	70.7 ± 7.0	117.3 ± 1.4	31.1 ± 3.1	1.44 ± 0.16	18.8 ± 1.8	25.0 ± 3.7	75.7 ± 6.8	115.2 ± 4.9
	35.2–35.8	21.7–25.8	15.0–17.5	65.5–80.6	115.7–118.2	27.4–34.3	1.29–1.60	15.4–21.6	19.1–31.4	64.8–87.1	108.6–118.9
	(n = 2)	(n = 4)	(n = 4)	(n = 4)	(n = 3)	(n = 4)	(n = 3)	(n = 11)	(n = 11)	(n = 11)	(n = 4)
Gorilla gorilla	45.5 ± 5.6	31.3 ± 4.0	25.5 ± 3.7	81.3 ± 4.7	119.0 ± 4.3	32 ± 6.2	0.92 ± 0.18	31.9 ± 4.0	38.3 ± 4.8	83.2 ± 4.0	–
	36.5–54.7	24.2–39.1	17.1–33.0	70.6–92.6	111.6–127.3	21.6–48.9	0.54–1.44	24.7–39.3	29.3–45.9	76.5–93.8	
	(n = 47)	(n = 47)	(n = 47)	(n = 47)	(n = 20)	(n = 47)	(n = 47)	(n = 47)	(n = 47)	(n = 47)	
Pan troglodytes	33.5 ± 2.1	23.4 ± 1.9	20.0 ± 1.3	85.9 ± 5.1	124.1 ± 4.6	27.3 ± 4.3	1.08 ± 0.20	23.4 ± 1.4	27.7 ± 1.9	85.0 ± 5.5	77.5 ± 11.9
	23.7–37.4	19.7–27.6	17.9–22.8	76.7–95.7	115–130.9	20.2–40	0.75–1.8	20.6–26.2	23.7–32.4	71.1–95.5	39.0–100.0
	(n = 42)	(n = 42)	(n = 42)	(n = 42)	(n = 20)	(n = 42)	(n = 42)	(n = 42)	(n = 42)	(n = 42)	(n = 56)
Homo sapiens	43.0 ± 4.3	31.5 ± 3.6	25.9 ± 4.4	82.4 ± 5.9	124.4 ± 3.8	33.4 ± 4.0	1.17 ± 0.14	25.7 ± 2.6	31.9 ± 3	80.8 ± 6.8	83.2 ± 16.6
	32.1–52.4	23.7–40.8	17.2–34.0	63.9–104.3	114.0–132.0	23.5–42.8	0.85–1.51	19.7–32.8	23.4–39.3	56.1–96.6	34.0–129.5
	(n = 195)	(n = 170)	(n = 170)	(n = 170)	(n = 100)	(n = 83)	(n = 83)	(n = 195)	(n = 195)	(n = 195)	(n = 105)
Australopithecus sp.[g]	33.2 ± 3.2	25.5 ± 3.2	17.8 ± 2.5	69.6 ± 6.9	120.3 ± 5.6	34.3 ± 7.6	1.29 ± 0.17	22.4 ± 3.8	29.9 ± 4.8	74.8 ± 3.5	108.7 ± 5.4
	28.6–40.2	21.1–32.4	13.8–24.9	55.5–81.2	112.5–134.0	22.2–43.1	1.12–1.59	16.9–29.6	21.8–38.9	66.4–81.7	104.0–116.3
	(n = 25)	(n = 23)	(n = 23)	(n = 23)	(n = 14)	(n = 10)	(n = 8)	(n = 19)	(n = 18)	(n = 18)	(n = 4)
Hominin indet.[h]	34.4 ± 1.9	26.4 ± 3.4	17.0 ± 2.3	65.0 ± 8.0	117.7 ± 4.6	35.4 ± 3.8	1.43 ± 0.15	22.2 ± 2.7	28.9 ± 1.95	77.1 ± 7.9	122.8
	33–35.7	21.9–30	15–20.5	54.6–71.9	115–123	30.1–39.7	1.30–1.66	18.8–27.1	26.8–31.3	61.4–86.6	
	(n = 2)	(n = 6)	(n = 6)	(n = 6)	(n = 3)	(n = 6)	(n = 5)	(n = 7)	(n = 7)	(n = 7)	(n = 1)
Early *Homo*[i]	40.1 ± 3.1	26.4 ± 2.8	20.2 ± 4.2	83.4 ± 2.7	124 ± 1.4	36.4 ± 1.8	1.36 ± 0.08	22.5 ± 1.6	28.2 ± 5.0	81.6 ± 12.3	106.7 ± 19.7
	37–43.1	24–30.3	13.2–24.2	80.0–85.9	123–125	35.1–37.6	1.30–1.41	20.4–24.2	20.9–31.9	69.6–97.6	92.7–120.6
	(n = 3)	(n = 4)	(n = 5)	(n = 4)	(n = 2)	(n = 2)	(n = 2)	(n = 4)	(n = 4)	(n = 4)	(n = 2)
Homo erectus[j]	43.5 ± 3.5	30.6 ± 2.2	24.5 ± 11.0	78.5 ± 1.3	110	46.3	1.61	25.6 ± 2.2	35.7 ± 2.7	71.8 ± 5.0	–
	41–46	29–32.1	13.4–39.3	77.6–79.4	(n = 1)	(n = 1)	(n = 1)	22.7–30.8	32.2–39.9	66.1–80.1	
	(n = 2)	(n = 2)	(n = 2)	(n = 2)				(n = 13)	(n = 13)	(n = 13)	
Middle Pleistocene Africa[k]	50.4 ± 7.9	41.4	39.3	84.6 ± 8.9	135	38.8 ± 2.3	1.07 ± 0.12	32.4 ± 3.4	40.8 ± 0.07	79.5 ± 8.5	–
	44.8–56.0	(n = 1)	(n = 1)	79.0–94.9	(n = 1)	37.2–40.4	0.99–1.15	30–34.8	40.7–40.8	73.5–85.5	
	(n = 2)			(n = 3)		(n = 2)	(n = 2)	(n = 2)	(n = 2)	(n = 2)	

[a] Fossil measurements taken on high quality casts and original specimens. Linear measurements are in mm, angular measurements are in degrees. Measurements are represented by mean ± std.dev., range, and sample size

[b] Neck length from intertrochanteric crest to the lateral edge of the head

[c] Neck length standardized by the subtrochanteric dimensions $\sqrt{(AP \times ML)}$

[d] Immature specimens

[e] Minimum head diameter

[f] Mature specimens: U.W. 101-002, U.W. 101-018, U.W. 101-271, U.W. 101-398, U.W. 101-421, U.W. 101-938, U.W. 101-1136, U.W. 101-1300, U.W. 101-1391, U.W. 101-1434, U.W. 101-1475, U.W. 101-1482

[g] U.W. 88-51 (MH2), U.W. 88-4,5,39 (MH1), A.L. 128-1, A.L.152-2, A.L. 211-1, A.L. 288-1, A.L. 333-3, A.L. 333-95, A.L.333-131, A.L. 827-1, MAK-VP 1/1, BOU-VP-12/1, KNM-WT 16002, MLD 46, Sts 14, StW 25, StW 99, StW 361, StW 392, StW 403, StW 479, StW 501, StW 522, StW 527, StW 598, SK 82, SK 97, SK 14024, SKX 3121, SKX 19, SWT1/LB-2, OH 20, OH 80, KNM-ER 1500, KNM-ER 1503, KNM-ER 1505 (includes material commonly classified as *Paranthropus*)

[h] KNM-ER 738, KNM-ER 815, KNM-ER 1463, KNM-ER 1465, KNM-ER 1809, KNM-ER 3728, KNM-ER 5880, StW 311

[i] KNM-ER 1472, KNM-ER 1475, KNM-ER 1481, KNM-ER 5881, OH 62

[j] KNM-ER 736, KNM-ER 737, KNM-ER 803, KNM-ER 1808, D4167, OH 28, BOU-VP 1/75, BOU-VP 19/63, Peking 1, Peking 4, Trinil 2, Trinil 3, Trinil 4, KNM-WT 15000

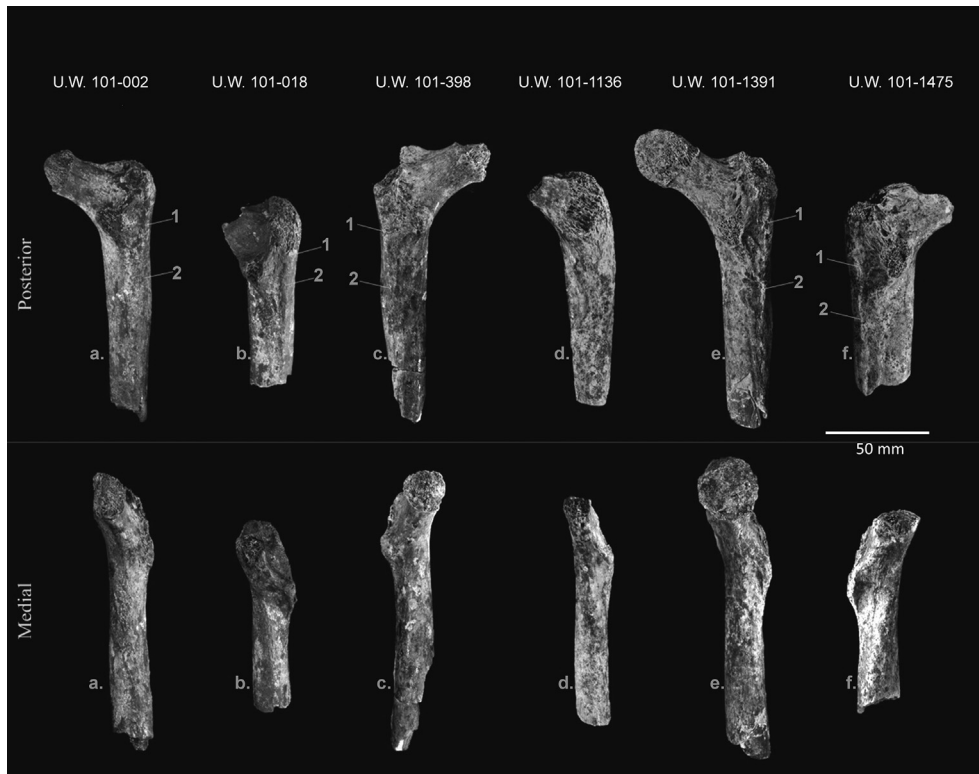[k] Berg Aukas, KNM-ER 999, Kabwe

Figure 4. Proximal femora of *Homo naledi*. From left to right: (a) U.W. 101-002, (b) U.W. 101-018, (c) U.W. 101-398, (d) U.W. 101-1136, (e) U.W. 101-1391, and (f) U.W. 101-1475. Note the presence of a third trochanter (1) on five of the six femora and the well-marked gluteal line for the distal insertion of m. gluteus maximus (2). In medial view, note the anteversion of the femoral neck as indicated by the angle formed by the longitudinal axis of the neck and the longitudinal axis of the proximal diaphysis.
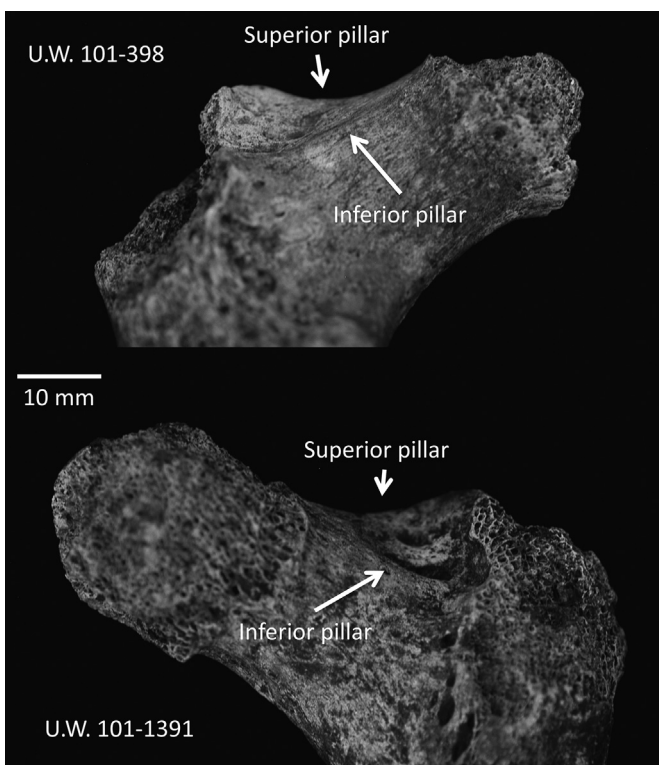

Figure 5. Proximal femora U.W. 101-398 and U.W. 101-1391, posterior view. Note superiorly, along the neck, the presence of two mediolaterally oriented pillars of bone and the resulting groove between the two. One pillar is more inferior and posterior, the other is more superior and anterior.

trochanter. The greater trochanter is complete though there are exposed trabeculae around the perimeter of the structure. Small patches of cortex are visible laterally and superiorly, allowing the general extent of the greater trochanter to be discerned. It is relatively low and exhibits weak lateral flaring from the axis of the shaft. The lesser trochanter is eroded, exposing internal trabeculae, however, it is visible in anterior view (dimensions approximately 16.0 SI and 10.9 mm ML). Inferomedial to the lesser trochanter is a prominent shelf that continues medially to a ridge of bone that extends inferolaterally from the lesser trochanter. The subtrochanteric region is platymeric. Along the posterolateral shaft is a prominent third trochanter, which descends inferiorly in the form of a gluteal line and lateral to which is a hypotrochanteric fossa. There is a pectineal line just medial to the third trochanter. The pectineal line and spiral line merge 24.3 mm from the distal break in the shaft. This line remains separate from the gluteal line in the preserved part of the shaft. At the break, the shaft is still somewhat platymeric: 22.3 mm ML and 18.4 mm AP. Here, the medial and lateral cortical shells are equally thick (6.5 mm).

U.W. 101-215 (Fig. 8) is a fragile and poorly preserved mature left distal femur preserving the distal and posterior part of the bone. The anterior portion of the femur has sheared away, exposing trabeculae throughout. The preserved subchondral bone is quite thin (<1 mm). The medial condyle was recovered in a fragmentary state and has been attached to the bone. In lateral view, the lateral condyle is flat and becomes convex posteriorly. The lateral edge is eroded, but there is a preserved pit for m. popliteus and a flexion groove that extends 11.9 mm posteriorly. The lateral condyle is a minimum of 20.6 mm wide; the height cannot be taken because of erosion. The lateral part of the intercondylar notch is preserved and is pocked with many vascular foramina. The anterior part of the intercondylar notch is smooth. The estimated biepicondylar width
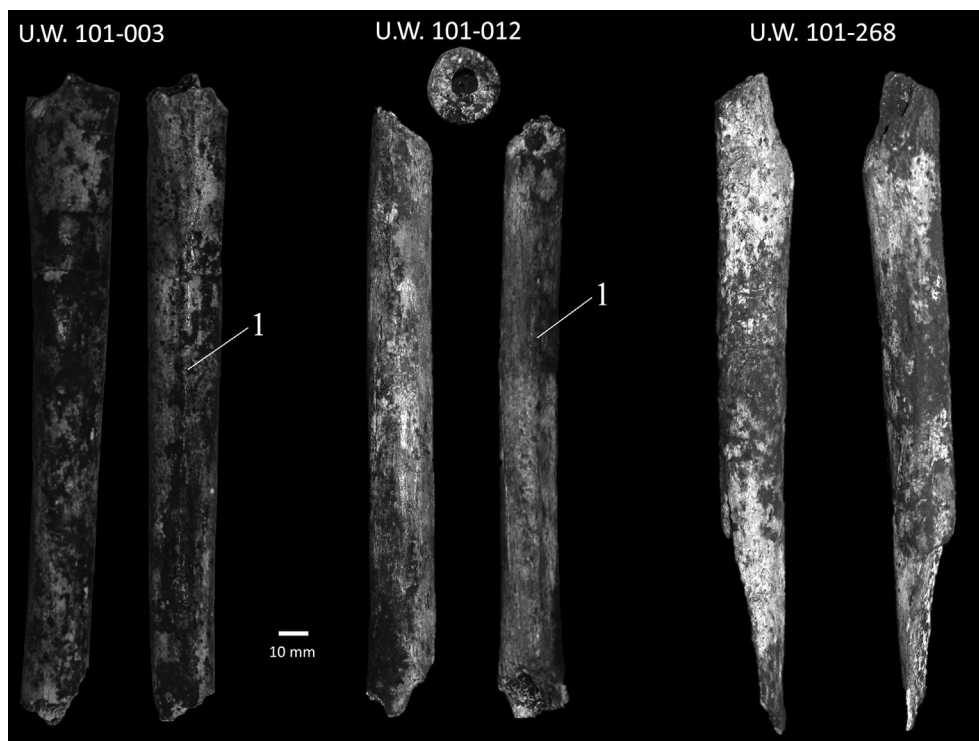
Figure 6. *Homo naledi* femoral shafts. Anterior view on the left, posterior view on the right. For U.W. 101-012, the proximal view of the break in the shaft is shown. Note the thick diaphyseal cortex. Also note the linea aspera (1) in U.W. 101-003 and U.W. 101-012.
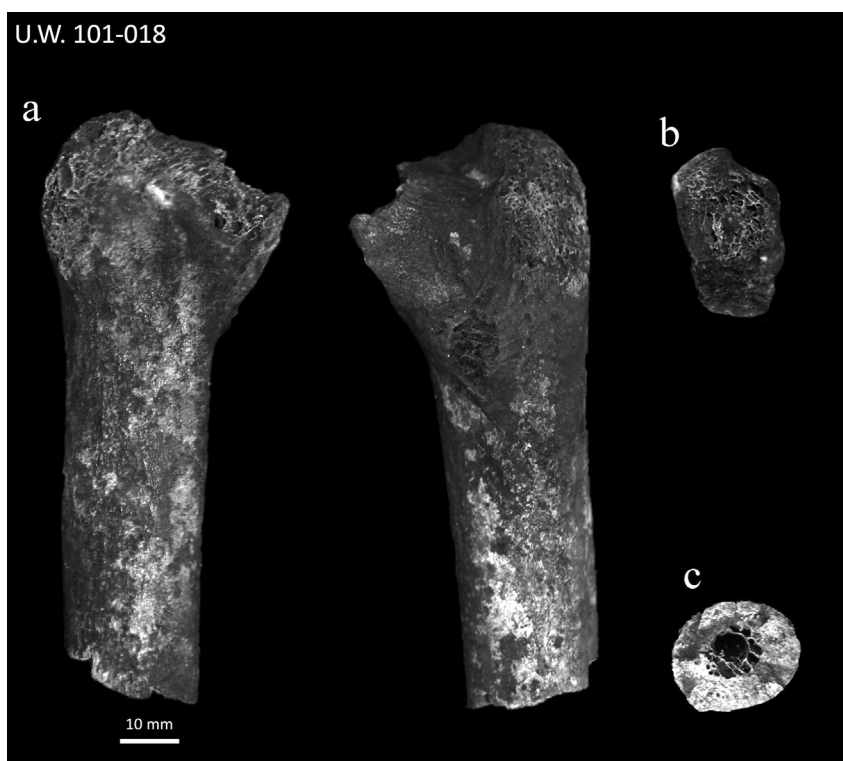

Figure 7. *Homo naledi* proximal femur U.W. 101-018 in (a) anterior (left) and posterior (right) view. (b) Medial view of a natural break in the neck. Left is anterior, right is posterior. Note the relatively thicker cortex inferiorly compared to superiorly. (c) Distal view of the distal break in the diaphysis. Note the thick cortex.

is 57.0 mm ML. There is a carrying angle, but its magnitude cannot be estimated because of the incompleteness of the diaphysis posteriorly and laterally and the imperfect match of the medial condyle with the diaphysis. The medial condyle is convex and is at least 18.8 mm ML. The intercondylar notch is 19.3 mm ML. The medial aspect of the condyle is eroded, but the lateral aspect has a
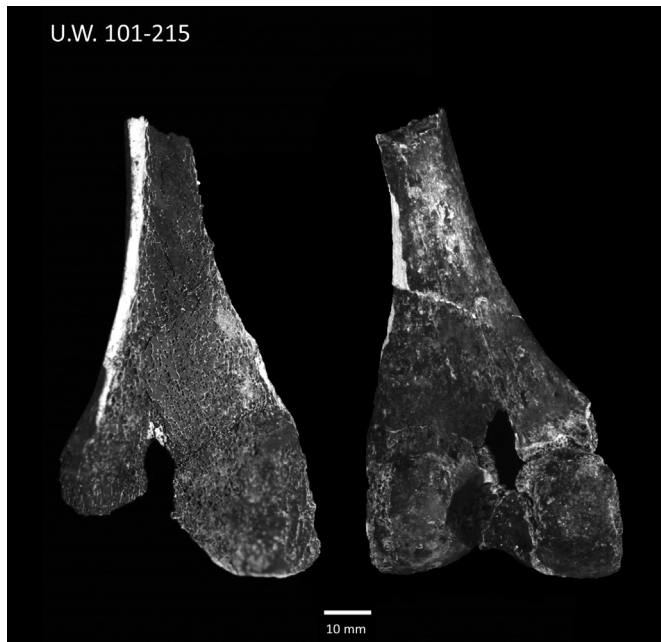
Figure 8. *Homo naledi* distal femur U.W. 101-215. Anterior view on the left, posterior view on the right. The medial condyle is attached to the specimen in posterior view, but not anterior view. Note the bicondylar angle observable in posterior view.

preserved edge. There are several fragments that may rejoin with this specimen.

U.W. 101-268 (Fig. 6) is a left femoral shaft. Proximally, the shaft is broken just inferior to the lesser trochanter and is platymeric. At the level of the proximal break the shaft exhibits torsion similar to that found in U.W. 101-003, which results in anteversion of the proximal part of the bone. At the ML narrowest part of the preserved shaft, the dimensions are 24.6 mm AP and 22.1 mm ML. Distally, the medial and posterior parts of the bone are not preserved at all. Anteriorly, the shaft is flat proximally and becomes rounded distally. There is heavy surface etching of the cortex making it difficult to discern any details of the bone. Posteriorly, there is a well-developed linea aspera that begins laterally and becomes centered distally. Proximomedially, there is a weak depression just medial to the linea aspera. Around midshaft, a rugosity, perhaps for the insertion of the adductors, appears medially and merges with the linea aspera that continues to descend distally.

U.W. 101-271 (Fig. 9) is a mature femoral head. Only the inferior part of the neck/head junction is preserved and covered with several foramina. Posteriorly there is minor surface abrasion exposing underlying trabeculae, though the cortex is generally well-preserved on this side of the bone. Superiorly and anteriorly the cortex is entirely stripped away, revealing trabeculae. Laterally, the head has sheared straight from the neck exposing trabeculae and only a very small (~15 mm ML) portion of the neck inferiorly.

U.W. 101-398 (Figs. 4c, 5) is a mature left femur preserving the femoral neck and proximal shaft. The head and greater trochanter have eroded away. The lesser trochanter is well-preserved. The primary fossil is U.W. 101-398; U.W. 101-226 is a 30 mm fragment refit to the distal shaft. Distally, the shaft extends further on the posterior than the anterior side due to a 21.4 mm SI piece of bone missing anteriorly. The shaft at the point of the distal break is 21.8 mm ML and 20.1 mm AP. The head is not preserved at all, though 23.5 mm SI, 20.5 mm AP, and 14.5 mm ML of a mass of trabeculae remains without any covering cortex delineating edges. However, there is a flaring, preserved ring of cortex, fenestrated with vascular foramina around the trabeculae, marking the neck/head junction. The neck is very well-preserved and is AP compressed. In lateral, medial, or superior view, the femoral head and neck deflect anteriorly. Posteriorly, there is a palpable and even visible obturator externus groove 3.6 mm wide (in the SI plane) running along the inferior margin of the neck. Posteriorly, there is a well-developed intertrochanteric crest connecting the lesser trochanter to the eroded greater trochanter: 17.6 mm of it is preserved SI. Superiorly, along the neck, there are two ML oriented pillars of bone positioned inferoposteriorly and superoanteriorly (Fig. 5). They are 9.1 mm away from one another and separated by a
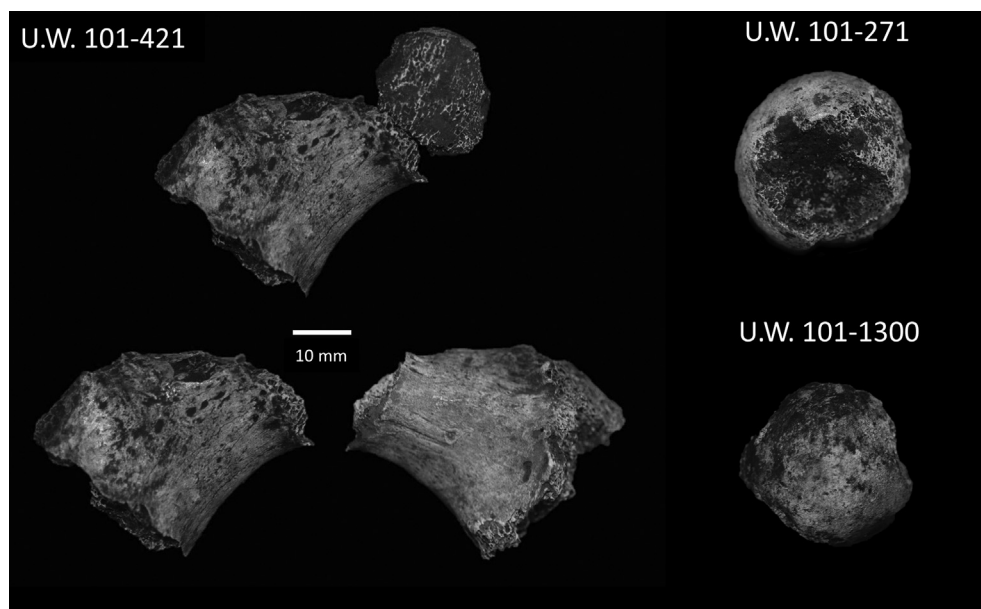

Figure 9. *Homo naledi* proximal femoral fragments: U.W. 101-271, U.W. 101-421, and U.W. 101-1300. U.W. 101-421 is shown at the top in anterior view with a conjoining fragment of femoral head. Below, the femoral neck and trochanteric region is shown in anterior (left) and posterior (right) views. To the right are two fragmentary femoral heads. Neither fossil conjoins with a *H. naledi* femoral neck, though each is complete enough to measure a femoral head diameter.

highly vascularized groove, especially laterally. Anteriorly, the neck is smooth and there is a very faint intertrochanteric line running superolaterally to inferomedially. Just lateral to the intertrochanteric line is a palpable depression (m. vastus lateralis). In anterior or posterior view, the inferior base of the greater trochanter flares laterally. The lesser trochanter measures 15.4 mm SI and 12.6 mm ML. It is positioned posteriorly, though in anterior view a small part of it can be seen medially. The center of the lesser trochanter is 36.1 mm from the inferolateral edge of the femoral head. Just inferior to the lesser trochanter, the shaft is platymeric. There is a strong bar of bone descending from the base of the lesser trochanter and continuing inferolaterally. Descending straight from the edge of the greater trochanter posterolaterally is a rugose gluteal line. Proximally, it is well-developed as a third trochanter. Lateral to the gluteal line is a region that becomes concave inferiorly (the hypotrochanteric fossa). Medial to the gluteal line is a well-developed pectineal line that merges with the gluteal line just medial to the inferior edge of the hypotrochanteric fossa. Medially, there is a detectable spiral line that runs inferior to the lesser trochanter. These muscle markings merge into a linea aspera inferiorly near a foramen that is just superior to the break in the shaft. Anteriorly, the shaft is convex; posteriorly, it is relatively flat.

U.W. 101-421 (Fig. 9) is a mature left proximal femur and partial head that are currently separate, but refit cleanly. The neck is well-preserved and is AP compressed. The greater trochanter has been sheared away and the point of break in the shaft does not preserve any of the lesser trochanter save for a very small portion of trabeculae superiorly. The head is badly damaged, with most of the cortex stripped except for some small patches superiorly and posteriorly. The preserved SI diameter from the preserved cortex of the superior head to the broken head/neck rim inferiorly is 33.5 mm, which is a minimum head diameter in this individual. Anteriorly, the neck is smooth, though a faint intertrochanteric line descends inferomedially. Just lateral to the intertrochanteric line is a concave depression for the m. vastus lateralis. Posteriorly, there is a faint but palpable obturator externus groove running along the inferior neck. Superiorly, there is a small trochanteric fossa preserved, which is filled with large vascular foramina. The head and neck exhibit torsion, resulting in a ML oriented posterior bar of bone more inferiorly positioned than the anterior bar of bone (which is superior).

U.W. 101-545 (Fig. 10) is a right distal femoral shaft. The anterior part of the shaft is well-preserved save for some longitudinal cracking. It is convex and flattens distally. At the far distal end of the preserved bone, there is the superior end of the sustrochlear hollow, which is depressed into the bone and filled with several foramina. It is slightly medial to center. The lateral shaft is a bit flatter than the medial, which remains convex. Posteriorly, there is less bone preserved, ca. 71.5 mm SI. Superiorly, a linea aspera descends distally 23.3 mm before splitting into lateral and medial supracondylar lines that gradually diverge down the shaft to the point of break. At the break, there are exposed trabeculae. Superiorly, the shaft is 22.4 mm AP and 20.5 mm ML. At the origin of the supracondylar lines, the shaft is 22.6 mm AP and 20.2 mm ML. There is no discernable waisting of the shaft.

U.W. 101-938 (Fig. 11) is an immature right femur preserving the femoral neck, the metaphyseal surface of the femoral head, part of the epiphyseal cap, some of the metaphyseal surface for the greater and lesser trochanters, and the majority of the shaft. There is erosional damage along the intertrochanteric crest and along the rims of the metaphyses. The fossil was found in four pieces. The most proximal piece is SI 88.4 mm from the proximal end of the eroded head to a jagged break in the shaft. Two shaft fragments approximately 63 mm and 100 mm in length each refit cleanly, as does a small (~24 mm) fragment of the popliteal surface of the posterior distal femur. The head is damaged around the margin of
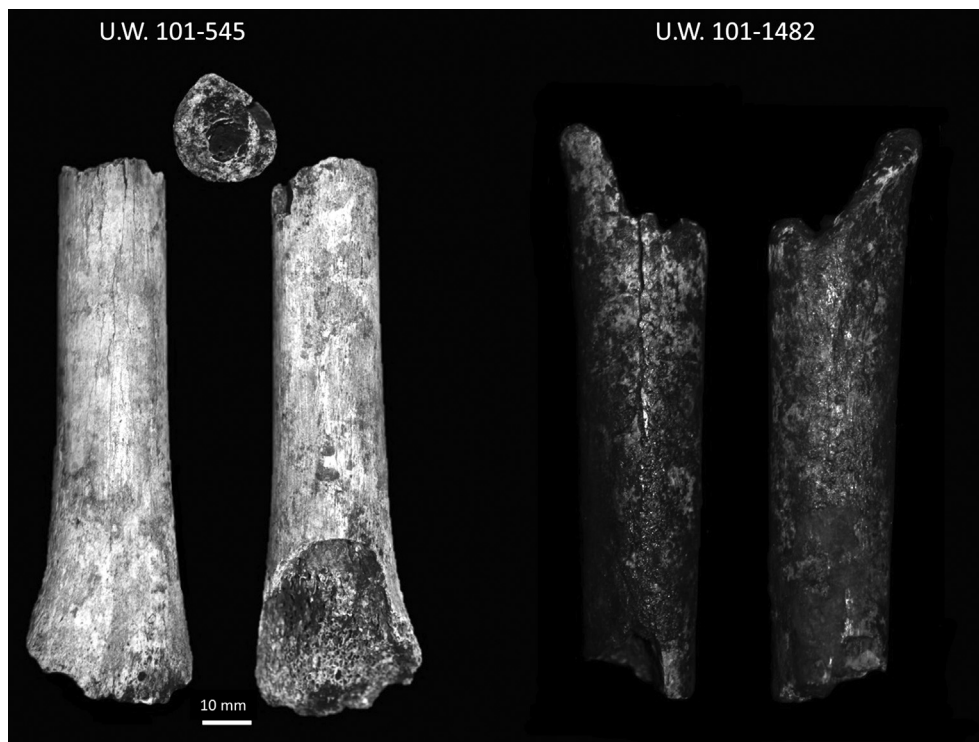

Figure 10. *Homo naledi* femoral shafts. Anterior view on the left, posterior view on the right. U.W. 101-545 is a right distal femoral shaft. Note the thick cortex at the proximal break and the presence of a weak pilaster in cross-section. Distally, U.W. 101-545 preserves evidence of a sustrochlear hollow, palpable just above the distal break. U.W. 101-1482 is a left femoral shaft fragment preserved from a break in the shaft inferior to the lesser trochanter to a break in the midshaft region.
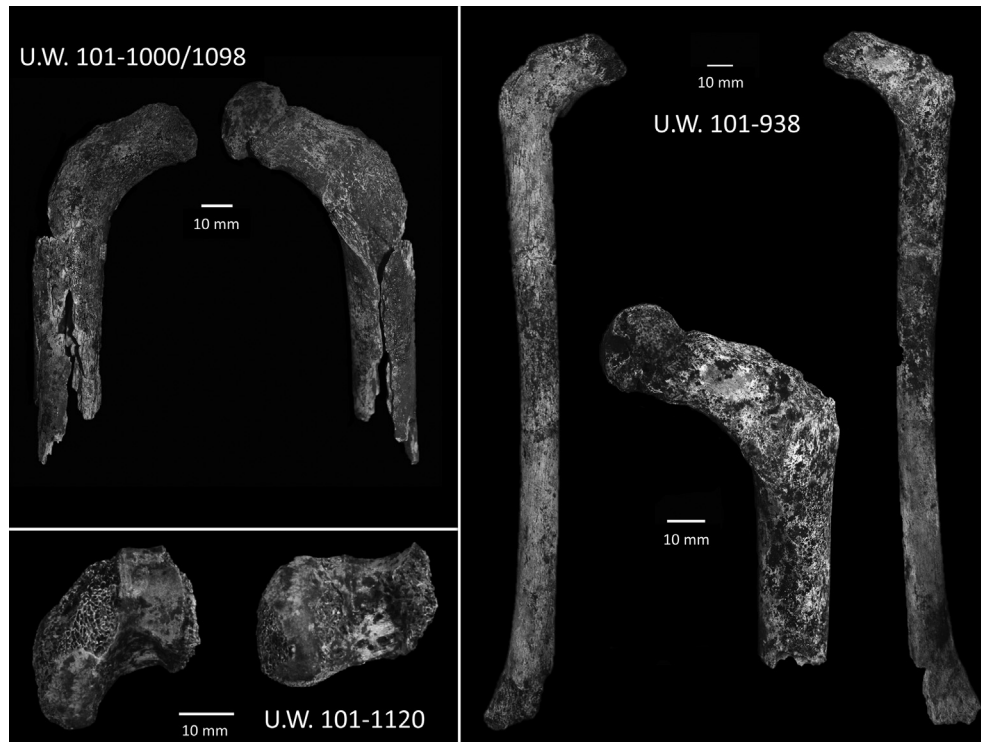
Figure 11. Immature femora of *Homo naledi*. Top left: U.W. 101-1000 and epiphyseal head U.W. 101-1098 in anterior (left) and posterior (right) view. The capital epiphysis is attached in just the posterior view. Top right: Completely preserved proximal portion and shaft of U.W. 101-938 in (left) anterior and (right) posterior view. At the center is just the proximal portion in posterior view with the attached capital epiphysis. Bottom left: the distal femoral epiphysis U.W. 101-1120 in anterior (left) and inferior (right) views. Note the rising lateral lip in inferior view.

the metaphysis, preserving a minimum of 20.6 mm AP, but without any delineating edges. The epiphyseal cap fits cleanly onto the metaphyseal surface. There is considerable erosion around the epiphyseal surface, but enough cortical bone is present to measure an approximate femoral head SI of 25.9 mm. The neck is well-preserved though there is some erosion of the cortical surface superiorly, exposing trabeculae. The neck is AP compressed. In lateral, medial, and superior view, the femoral head and neck deflect anteriorly. The posterior neck is smooth and there is a barely detectable obturator externus groove running along the inferior margin of the neck. Superiorly, along the neck, there are two weakly developed ML running pillars of bone, contributing to head/neck torsion relative to the long axis of the shaft. There is also considerable femoral anteversion relative to the linea aspera. Anteriorly, the neck is smooth, without any evidence of an inter-trochanteric line. Laterally and superiorly is the surface for the apophysis of the greater trochanter. It is inferolaterally angled relative to the superior aspect of the neck. The metaphysis for the greater trochanter advances quite medially and is only 16.5 mm ML from the most lateral metaphyseal surface for the femoral head. In posterior view, there is weak lateral flare at the base of the greater trochanter. The lesser trochanter is preserved medially with a small patch (5.9 mm SI, 4.0 mm ML) of metaphyseal surface surrounded laterally and distally by exposed trabeculae. The lesser trochanter is positioned posteriorly, though in anterior view a small part of it can be seen medially, as is the case with most other femora in the assemblage. The center of the lesser trochanter is 28.6 mm from the inferolateral edge of the femoral head. Just inferior to the lesser trochanter, the shaft is platymeric. Descending from the base of the lesser trochanter and continuing infer-olaterally to form the pectineal line is a prominent bar of bone. The pectineal line merges distally (~38 mm from the base of the lesser trochanter) with the gluteal line. The two are separated by a groove

that narrows inferiorly. Lateral to the gluteal line is a flattened region, the hypotrochanteric fossa. Anteriorly, the shaft is convex and there are several longitudinal cracks along the shaft, though they do not alter the anatomy of the bone. Along the posterior shaft is a linea aspera that is most strongly developed from the midshaft distally. Here, the linea aspera weakens and splits into barely detectable supracondylar lines. At approximately midshaft, the shaft is 17 mm AP and 15 mm ML. The narrowest ML region of the shaft is 14.6 mm ML and only 15 mm distal to the midshaft, indi-cating femoral wasting.

U.W. 101-1000/1098 (Fig. 11) is an immature right proximal fe-mur preserving the metaphyseal surface of the head, the neck, and a fragmentary proximal shaft. The metaphyseal surface for the greater trochanter is badly eroded, though there is a small patch of undifferentiated bone anteromedially. The metaphysis for the head is well-preserved. There is some erosion around the perimeter, though a maximum AP dimension of 25.7 mm can be measured, which matches the 25.7 mm AP of the associated epiphyseal head (U.W. 101-1098). There are metaphyseal grooves and furrows around the perimeter and a pit located centrally. The posterior neck is smooth and preserves about 19 mm of cortex from the lateral edge of the head to a break in the bone that exposes trabeculae. There is no evidence for an obturator externus groove. Anteriorly, the neck is better preserved and is smooth, grading laterally into a small pit for m. vastus lateralis. An intertrochanteric line is not present. The neck is AP compressed. Superiorly, the neck is 14.6 mm long, from the lateral edge of the head metaphysis to the medial edge of the metaphysis for the greater trochanter. Only a small patch (14.5 mm ML, 8.8 mm AP) of the metaphyseal surface of the greater trochanter is preserved and is moderately angled infer-olaterally relative to the long axis of the neck. There is a 66.5 mm piece of the lateral shaft that conjoins posterolaterally to U.W. 101-1000, but anteriorly there is no clean fit.

U.W. 101-1120 (Fig. 11) is an immature left distal femoral epiphysis. It is quite fragmentary with exposed trabeculae medially. The lateral condyle was not recovered. 33.5 mm ML of the epiphysis is preserved. There is preserved cortex along the inferior rim of the medial condyle, which is convex. The intercondylar notch is reasonably well-preserved and pocked with vascular foramina. In inferior view, it is 13.3 mm SI, but the ML diameter cannot be assessed because the lateral condyle was not recovered. The patellar surface has preserved cortex 13.5 mm ML and is moderately concave medially, but exhibits the beginning of a lateral patellar lip, especially in inferior view. While there is topography to the metaphyseal surface, it lacks a deep ML groove.

U.W. 101-1136 (Fig. 4d) is a right proximal femur preserved from a break along the superior neck and head to a break in the shaft. The head, greater trochanter, and lesser trochanter are not preserved and there are exposed trabeculae in those regions. The shaft has some exfoliated cortex and cracking throughout. Because of the flaking of the cortex, it is difficult to discern any muscle markings along the shaft, with the possible exception of a hypotrochanteric fossa along the posterolateral part of the shaft. The neck is poorly preserved. The SI dimensions are unknown because of damage superiorly. Features of hominin neck anatomy, like the obturator externus groove or the intertrochanteric line, are not detectable because of surface erosion. The neck is anteriorly shifted relative to the shaft and the neck has experienced torsion. The subtrochanteric dimensions are platymeric. At the point of the distal break in the shaft, the dimensions are 17.3 mm AP and 17.1 mm ML.

U.W. 101-1300 (Fig. 9) is an unsided femoral head. It is sheared laterally. It is unclear if the anterior part of a right or the posterior part of a left femoral head is preserved. The fovea is well-preserved and is 8.6 mm SI and 6.6 mm ML. It is deeply pitted with several foramina in the interior.

U.W. 101-1391 (Figs. 4e, 5) is a mature right femur preserving part of the head, the femoral neck, some of the greater and lesser trochanters, and a large portion of the proximal shaft. There is erosional damage around the perimeter of the femoral head, along the greater trochanter, and on the lesser trochanter, exposing trabecular bone. The bone was recovered in two pieces, separated by a break below the lesser trochanter; the two pieces of the proximal femur and the shaft are glued back together cleanly. At the distal break, a triangular fragment has been glued back into place. The head is damaged circumferentially. Only a small patch of cortex is preserved medially and another small patch posteriorly, preventing an estimate of femoral head diameter. The neck is well-preserved and AP compressed. In lateral, medial, or superior view, the femoral head and neck deflect anteriorly. Posteriorly, there is a detectable obturator externus groove running along the inferior margin of the neck. Superiorly along the neck there are two ML oriented pillars of bone positioned inferoposteriorly and superoanteriorly (Fig. 5), resulting in head/neck torsion relative to the long axis of the shaft. Anteriorly, there is a weakly developed intertrochanteric line descending from a palpable femoral tubercle. It continues around the inferior part of the neck and descends as the spiral line down the posterior shaft. Superiorly, the neck grades into a trochanteric fossa that is angled towards the posterior part of the bone. There are two large foramina medial to a pit. In posterior view, the shaft begins to flare laterally at the base of the greater trochanter. The lesser trochanter is eroded, though the cortical ring around the trabeculae indicates that the lesser trochanter would have been about 13.3 mm SI and 10 mm ML. The lesser trochanter is positioned posteriorly, though in anterior view a small part of it can be seen medially. The center of the lesser trochanter is 35.8 mm from the inferolateral edge of the femoral head. Medial to the lesser trochanter, there is a strong ridge of bone producing an indentation between the projecting lesser trochanter and the spiral line. Just

inferior to the lesser trochanter, the shaft is platymeric. A prominent bar of bone descends from the base of the lesser trochanter and continues inferolaterally to form the pectineal line. The pectineal line merges distally (~42 mm from the base of the lesser trochanter) with the gluteal line and the beginnings of the linea aspera are detectable at the distal break in the shaft. Proximally, the gluteal line is well-developed as a third trochanter. The pectineal line and the gluteal line are separated by a groove that narrows inferiorly. Lateral to the gluteal line is a flattened region, the hypotrochanteric fossa, inferior to which is a laterally bulging rugosity. Anteriorly, the shaft is convex. The shaft at the point of break is 19.5 mm ML and 22.5 mm AP. Here, the medial cortex is thicker (6.3 mm) than the lateral cortex (4.6 mm).

U.W. 101-1475 (Fig. 4f) is a mature left proximal femur preserving the neck, eroded greater trochanter, and proximal shaft. The neck is broken in a manner that preserves the inferior, anterior, and posterior portions, but the superior and medial aspect is missing. A break in the neck reveals internal trabeculae and thick cortex along the inferior margin. There is erosion around the perimeters of the lesser and greater trochanters revealing trabecular bone. Posteriorly along the neck there is a weakly developed obturator externus groove (especially laterally). Anteriorly, the neck is quite smooth with little evidence for an intertrochanteric line. Inferior to the neck, there is the start of a palpable spiral line that twists posteriorly and inferiorly. It merges with the pectineal line 25.2 mm inferior to the lesser trochanter. The greater trochanter is badly damaged, though inferiorly it exhibits weak lateral flaring from the axis of the shaft. It is separated from the lesser trochanter by an intertrochanteric crest that preserves only 15.4 mm in the SI plane of the cortex. The lesser trochanter is eroded, though it can be seen projecting medially in anterior view and the dimensions can be measured (16.6 mm SI and 12.1 mm ML). Just inferior to the lesser trochanter, the shaft is platymeric. Medial to the lesser trochanter there is a prominent pillar of bone that runs proximoanteriorly to distoposteriorly and contributes to the anterior torsion of this proximal femur. Along the posterolateral shaft is a prominent third trochanter, which descends inferiorly in the form of a gluteal line and lateral to which is a hypotrochanteric fossa. There is a pectineal line just medial to the third trochanter. At the point of break, the shaft is platymeric: 26.3 mm ML and 20.3 mm AP. Here, the medial cortex is thicker (9.7 mm) than the lateral cortex (7.3 mm).

U.W. 101-1482 (Fig. 10) is a left femoral shaft fragment preserved from a break in the shaft inferior to the lesser trochanter to a break in the midshaft region. The proximal break is oblique, running proximomedial to distolateral. The subtrochanteric region is platymeric. The cortex is roughened making identification of muscular insertions difficult, however, there is a detectable spiral line descending from the lesser trochanteric region and a faint impression of the pectineal line. Distally, a well-developed linea aspera descends the length of the remainder of the shaft. At the break in the shaft, the bone is 23.2 mm AP and 25.1 mm ML. Here, the medial cortex is thicker (8.4 mm) than the lateral cortex (7.6 mm).

3.2. Patella

Homo naledi patella dimensions are listed in Table 4, with material depicted in Figure 12.

U.W. 101-852 (Fig. 12) is a right patella preserving some of the base, the anterior surface, and the posterior contact with the distal femur, especially laterally. The medial side of the bone and the apex were not recovered, making height and length measurements impossible. However, the bone is 18.3 mm thick AP. The minimum SI diameter from the tip of the base to the break inferiorly is 24.9 mm. The minimum distance ML from the lateral edge to a

Table 4
Comparative patella dimensions.[a]

Specimen/Species	ML width	SI height	AP thickness	AP/ML × 100
U.W. 101-852	–	–	18.3	–
U.W. 101-1404	30.0	–	16.2	54.0
U.W. 101-1639	–	–	14.9 (min)	–
Gorilla gorilla	38.1 ± 5.0	35.6 ± 4.4	16.8 ± 2.4	44.1 ± 2.4
	32.3–46.4	30.3–42.1	13.5–20	41.4–47.9
	(n = 10)	(n = 10)	(n = 10)	(n = 10)
Pan troglodytes	24.4 ± 1.6	26.2 ± 2.4	10.2 ± 1.5	42.0 ± 5.8
	21.5–26.3	24.2–30.8	8.4–12.2	35.3–49.4
	(n = 9)	(n = 9)	(n = 9)	(n = 9)
Homo sapiens	37.7 ± 4.1	36.8 ± 4.3	18.1 ± 1.8	48.0 ± 3.3
	32.0–52.2	31.7–54.5	14.3–22	41.6–55.7
	(n = 53)	(n = 37)	(n = 53)	(n = 53)
Australopithecus sediba[b]	26.8	24.7	13.1	48.9
Australopithecus robustus[c]	30.1	–	13.3	44.2
Homo floresiensis[d]	30.7	32.3	12.2	39.7
Homo antecessor[e]	36.2 ± 0.35	37.0 ± 0.14	19.2 ± 0.28	53.0 ± 0.99
	36.1–36.3	36.7–37.2	19.0–19.4	52.3–53.7
	(n = 2)	(n = 2)	(n = 2)	(n = 2)
Homo heidelbergensis[e]	47.9 ± 3.0	43.7 ± 2.0	23.1 ± 1.7	48.2 ± 1.2
	42.6–51.3	40.6–46.6	20.0–25.0	46.9–50.0
	(n = 5)	(n = 5)	(n = 5)	(n = 5)
Homo neanderthalensis[e]	47.2 ± 4.2	43.5 ± 3.9	22.7 ± 3.2	48.3 ± 2.6
	39.0–56.5	36.0–51.0	17.0–28.5	43.6–53.5
	(n = 14)	(n = 15)	(n = 13)	(n = 12)

[a] Measurements taken on original specimens unless noted otherwise
[b] U.W. 88-79,100
[c] SKX 1084
[d] LB1/10, LB1/11
[e] Data from Carretero et al. (1999)

break medially is 27.8 mm. Posteriorly, the facet for the distal femur is strongly ML curved. From the height of the femoral surface, the lateral facet strongly slopes anteriorly and is moderately concave at the most lateral point. The lateral facet is 20.7 mm ML. Medially, the facet is preserved for only 7.1 mm and is flat, with a less steep slope. Internally, the patella is filled with trabeculae that are exposed medially and inferiorly. Proximally, the base is relatively smooth and somewhat eroded along the most proximal rim. It is deflected posteriorly relative to the anterior aspect of the patella, which is vascular and has several vertical striations.

U.W. 101-1404 (Fig. 12) is a right patella preserving some of the base, the anteromedial surface, and a small portion of the lateral femoral surface. A piece of the patellar surface is broken away from the anterior part of the bone, but the two fragments refit. Much of the lateral side of the bone and the apex were not recovered, preventing an SI diameter measure. The ML length of the specimen is ~30 mm and the AP thickness is 16.2 mm. The minimum SI diameter from the tip of the base to the break inferiorly is 26.0 mm, though this patella would have been taller. Posteriorly the facet for the distal femur is preserved only laterally. It rises from a high central region and slopes anteriorly, forming a rather flat ML facet. The lateral facet preserves 21.3 mm ML and 16.2 mm SI. Internally, the fragment is filled with trabeculae. Proximally, the base deflects posteriorly relative to the anterior aspect of the patella, which has several vertical striations.

3.3. Tibia

Homo naledi tibia dimensions are listed in Table 5, with material depicted in Figures 13 – 16 (3D surface scans available at www.morphosource.org).

U.W. 101-213 (Fig. 13) is a right proximal tibial shaft fragment. It is constituted by the association of three fragments: U.W. 101-213, U.W. 101-214, and U.W. 101-312. The anterior part of the bone, including the tibial tuberosity, has been stripped away. Posteriorly, the soleal line descends superolaterally to inferomedially across the shaft for 66 mm. The vertical line is not visible. There is a depression laterally between the soleal line and the interosseous crest (mm. flexor digitorum longus and tibialis posterior). The anterior
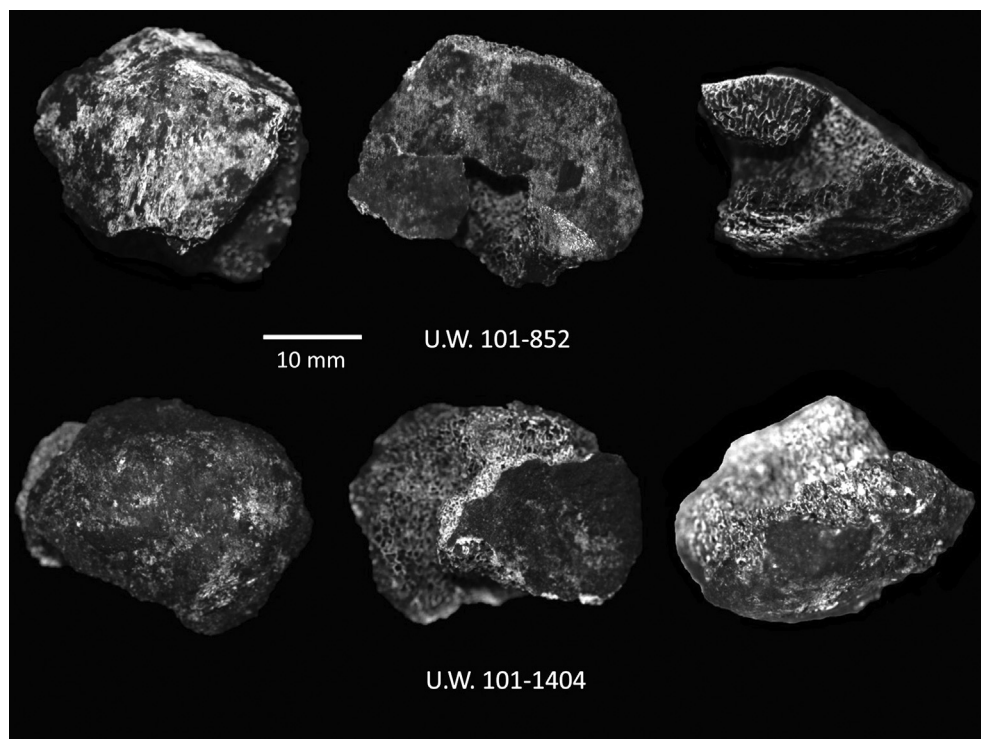

Figure 12. *Homo naledi* patellae. From left to right: anterior, posterior, and superoinferior (transverse plane section) view. Note the anteroposterior thickness in the SI view.

Table 5
Comparative tibia dimensions.[a]

Specimen/Species	Diaphysis						Distal metaphysis		Talar articular surface					
	ML at nutrient foramen	AP at nutrient foramen	Platycnemic index at nutrient foramen (ML/AP) × 100	Midshaft ML	Midshaft AP	Midshaft index (ML/AP) × 100	AP	ML	AP lateral	AP midpoint	AP medial	ML anterior	ML midpoint	ML posterior
U.W. 101-420	–	–	–	–	–	–	30.3	–	20.0	19.5	17.2	–	19.4	–
U.W. 101-484	18.0	27.1	66.4	17.6	25.0	70.4	–	–	–	–	–	–	–	–
U.W. 101-711	–	–	–	–	–	–	29.5	–	–	–	–	–	–	–
U.W. 101-973	18.0	27.1	66.4	–	–	–	–	–	–	–	–	–	–	–
U.W. 101-996[b]	14.7	21.3	69.0	–	–	–	19.8	21.2	–	–	–	–	–	–
U.W. 101-1070[b]	14.3	21.3	67.1	14.1	20.0	70.5	–	21.7	–	15.4	14.1	–	–	–
U.W. 101-1262	–	–	–	–	–	–	–	–	–	–	14.1	–	–	–
U.W. 101-1416	–	–	–	–	–	–	25.4	–	15.4	–	–	18.7 (est.)	17.1	15.0
Homo naledi[c]	18.0	27.1	66.4	17.6	25.0	70.4	28.4 ± 2.6	–	17.7	19.5	15.7	18.7	18.3	15.0
	18.0–18.0	27.1–27.1	66.4–66.4	(n = 1)	(n = 1)	(n = 1)	25.4–30.3		15.4–20.0	(n = 1)	14.1–17.2	(n = 1)	17.1–19.4	(n = 1)
	(n = 2)	(n = 2)	(n = 2)				(n = 3)		(n = 2)		(n = 2)		(n = 2)	
Gorilla gorilla	24.1 ± 1.1	35.8 ± 4.0	67.9 ± 7.5	23.7 ± 2.2	31.7 ± 4.0	75.2 ± 6.1	28 ± 4.6	44.1 ± 7	24.7 ± 3.1	27.7 ± 3.7	26.4 ± 3.3	38.7 ± 4.5	29 ± 3.8	21.6 ± 3.3
	23–25.5	28.4–40	58.1–81.1	20.6–25.8	25.1–37.1	68.3–82.9	20.1–38.1	31.3–56.8	18.5–30.5	22.0–36.0	18–32.5	30.3–45.7	23.8–37.2	15.5–30.1
	(n = 6)	(n = 6)	(n = 6)	(n = 6	(n = 6)	(n = 6)	(n = 44)	(n = 44)	(n = 44)	(n = 44)	(n = 44)	(n = 44)	(n = 44)	(n = 44)
Pan troglodytes	18.0 ± 2.0	28.1 ± 3.5	64.3 ± 5.5	16.6 ± 1.5	24.4 ± 2.9	68.3 ± 6.4	21.1 ± 1.8	30.6 ± 3.1	19.2 ± 1.6	20.8 ± 1.9	18.7 ± 1.7	27.3 ± 2.1	21.4 ± 1.5	17.6 ± 1.7
	14.7–20.3	23.8–33.2	55.7–73.0	14.8–19.3	20.3–29.3	57.6–77.2	17.6–25.9	25.1–40	16.3–21.6	16.7–24.5	15.2–22	24.3–35.9	18.5–27	14.3–21
	(n = 10)	(n = 10)	(n = 10)	(n = 10)	(n = 10)	(n = 10)	(n = 49)	(n = 49)	(n = 49)	(n = 49)	(n = 49)	(n = 49)	(n = 49)	(n = 49)
Homo sapiens	23.1 ± 3.1	30.7 ± 4.4	75.2 ± 5.2	22/4 ± 2.4	30.6 ± 2.4	73.4 ± 6.1	30.9 ± 3.6	37.6 ± 3.9	28.4 ± 2.6	27.0 ± 2.6	23.7 ± 2.2	31.9 ± 2.8	28.4 ± 2.4	25.6 ± 2.2
	19.2–29.5	25.2–39.4	64.8–84.7	18–26.7	23.2–34.6	64.3–86.9	23.2–40	29.3–46.8	22.9–24.9	21.8–35	18.7–30.1	25.5–38.8	23.2–34.7	20.3–31.4
	(n = 23)	(n = 23)	(n = 23)	(n = 23)	(n = 23)	(n = 23)	(n = 79)	(n = 79)	(n = 145)	(n = 145)	(n = 145)	(n = 145)	(n = 145)	(n = 145)
Australopithecus sp.[d]	15.0 ± 0.5	22.5 ± 0.1	66.7	–	–	–	26.7 ± 3.6	30.1 ± 3.5	21 ± 2.5	20.1 ± 2.3	17.4 ± 1.7	22.7 ± 2.9	20.1 ± 2.9	18.8 ± 2.6
	14.7–15.3	22.4–22.5	64.7–68.4				21.3–33.4	24.5–35.6	18.6–25	17.2–23.9	14.6–20.4	19.2–28.3	17.2–25.4	14.4–23.2
	(n = 2)	(n = 2)	(n = 2)				(n = 10)	(n = 10)	(n = 11)	(n = 10)	(n = 11)	(n = 12)	(n = 13)	(n = 12)
Early *Homo*[e]	15.6	25.5	61.2	14.5	22.2	65.3	29.6 ± 5.3	32.7 ± 8.1	22.7 ± 2.4	20.5 ± 3.9	19.3 ± 2.6	24.8 ± 3.0	23.0 ± 3.0	18.8 ± 3.0
	(n = 1)	(n = 1)	(n = 1)	(n = 1)	(n = 1)	(n = 1)	27–38.4	27.0–38.4	20.1–24.9	16.3–24.0	16.4–21.3	21.6–27.4	19.8–25.7	16.5–22.2
							(n = 3)	(n = 2)	(n = 3)	(n = 3)	(n = 3)	(n = 3)	(n = 3)	(n = 3)
Homo erectus[f]	23.0	32.0	71.2	19.7 ± 1.2	26.0 ± 2.2	76.2 ± 9.3	35.7	35.3 ± 0.8	31.5 ± 0.4	28.9 ± 1.1	25.3 ± 2.2	30.7 ± 1.9	27.4 ± 0.9	25.9 ± 0.5
	(n = 1)	(n = 1)	(n = 1)	18.0–20.4	24.0–28.6	66.7–85.0	(n = 1)	34.7–35.8	31.2–31.7	28.1–29.7	23.7–26.8	29.3–32.0	26.8–28.0	25.5–26.2
				(n = 4)	(n = 4)	(n = 4)		(n = 2)	(n = 2)	(n = 2)	(n = 2)	(n = 2)	(n = 2)	(n = 2)

[a] Measurements taken on high quality casts and original specimens. Linear measurements are in mm. Measurements are represented by mean ± std.dev., range, and sample size
[b] Immature specimens
[c] Mature specimens: U.W. 101-420, U.W. 101-484, U.W. 101-711, U.W. 101-973, U.W. 101-1262, U.W. 101-1416
[d] A.L 288-1AQ, A.L 129-1b, A.L 333-6, A.L. 333-7, A.L. 545-3 from Ward et al., 2012, KNM-KP 29285, StW 181, StW 358, StW 389, StW 515, U.W. 88-21 (MH4), U.W. 88-97 (MH2), KNM-ER 1500, KNM-ER 2596 (includes material commonly classified as *Paranthropus*)
[e] OH35a, KNM-ER 1481; StW 567
[f] D3901 from Lordkipanidze et al., 2007, KNM-ER 741, KNM-ER 803b, KNM-WT 15000
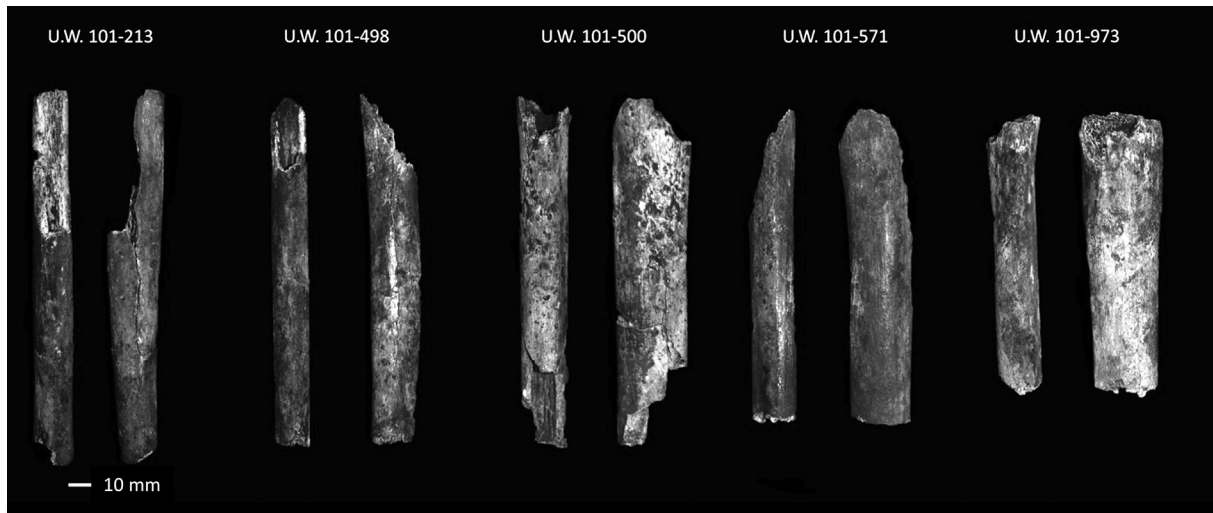
Figure 13. *Homo naledi* tibial shafts. Left anterior view, right medial view. Note the platycnemic shape in all tibiae.

border curves from anteromedially to distolaterally and is rounded. Distally the diaphysis flares in anterior and posterior view and the cross-section is less triangular than it is proximally. At the proximal point of the break (where the soleal line is no longer visible), the bone is 22.7 mm AP and 16.8 mm ML.

U.W. 101-420 (Fig. 14) is a mature left distal tibia preserved from the rims of the tibial plafond to a break in the tibial shaft. There is damage to the distomedial part of the metaphysis, though it is AP expanded. The tibiotalar articular surface is well-preserved, though the medial malleolus has been sheared away. There is a gentle AP-oriented keel dividing the facet into a lateral (11.9 mm ML) and medial (9.5 mm minimum ML) region. The lateral part of the facet is slightly concave ML and more concave AP; the medial part is flat ML and concave AP. In the coronal plane, the tibiotalar articular surface is orthogonal to the long axis of the tibial shaft, as is common in bipedal hominins. Anteriorly, the rim of the tibiotalar surface possesses a small squatting facet that is 3.9 mm SI. Its ML extent is unclear because the medial malleolus has been sheared away from
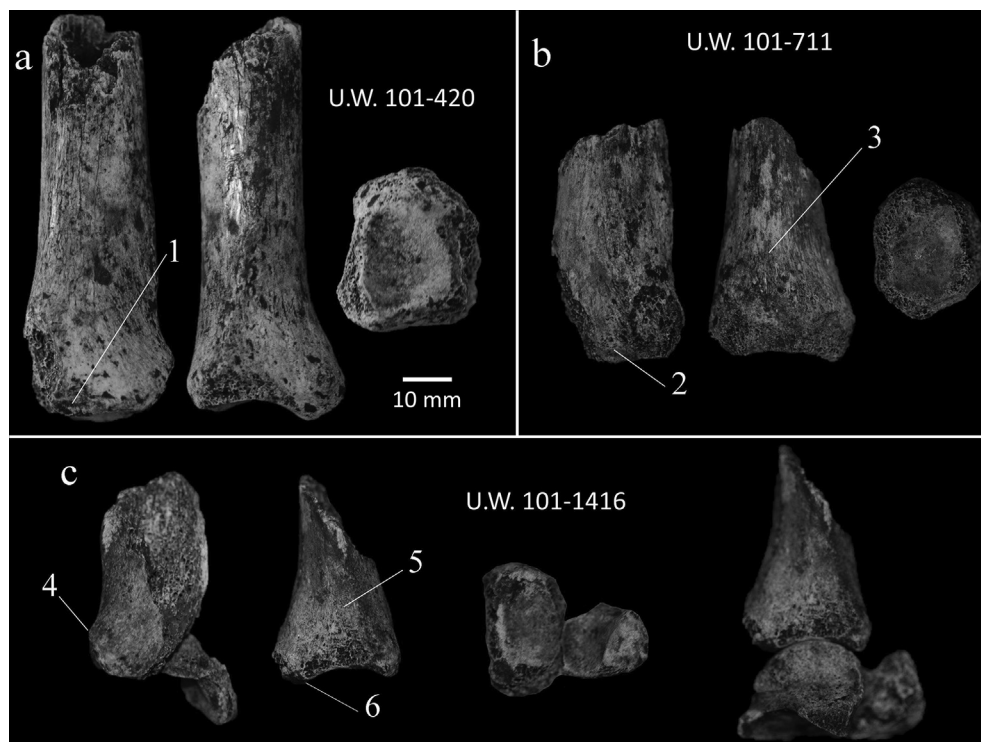
Figure 14. Distal tibia of *Homo naledi*. (a) Left distal tibia. Left anterior view, center lateral view, right distal view. Anteriorly, the rim of the tibiotalar surface possesses a small squatting facet (1). (b) Left distal tibia. Left anterior view, center lateral view, right distal view. Note the squatting facet visible in anterior view (2) and the strong interosseous crest in lateral view (3). (c) Right distal tibia. From left to right: anterior view, lateral view, distal view, and lateral view articulated with talus U.W. 101-1417, which belongs to foot 1 (Harcourt-Smith et al., 2015). Note the large laterally positioned anterior tubercle for the anterior tibiofibular ligament (4). Laterally, there is a strong interosseous crest (5) descending anterodistally. Note in lateral view (6) the posterior rim of the tibial plafond that is more distally projecting than the anterior rim.

the bone, taking with it a portion of the anteromedial shaft. Anteromedially, a pillar of bone extends proximolaterally to the break in the shaft. Anteriorly, the break is 59.7 mm from the tibiotalar articular surface. At this point of the shaft, the dimensions are 21.7 mm AP and 20.4 mm ML. Medially, the shaft is flat and bordered anteriorly and posteriorly by thickened bony pillars. The posterior shaft is convex with a thick pillar of bone running down its length. Laterally, there is a well-preserved and large posterior tuberosity for the posterior tibiofibular ligament. Laterally, the crest for the interosseous membrane descends anterodistally and terminates in a small anterior tubercle. This crest is well-marked, elevated, and rough. There is no detectable posterior component to this crest. The fibular facet has eroded away. In lateral view, the posterior rim of the tibial plafond is more distally projecting than the anterior rim.

U.W. 101-484 (Fig. 15) is a mature right tibia preserved from a break in the proximal shaft just proximal to the tibial tuberosity to a small preserved patch of the talar articular surface. The tibial tuberosity itself is not preserved, but the vertical striations just distal to it are. The shaft is reasonably well-preserved, though there is post-mortem damage along its length. The shaft was discovered in three pieces, two similarly sized proximal elements and a longer distal piece: individual lengths are approximately 93 mm for the proximal portion, 85 mm for the middle fragment, and 115 mm for the distal fragment. Each contacts the previous piece cleanly and has left a crack around the perimeter of the shaft. Anteriorly, the shaft is dominated by a sharp crest that is smooth distally and grades into the base of the tibial tuberosity proximally. At the base of the tuberosity, the shaft is 33.1 mm AP and 20.2 mm ML. In medial or lateral view, the posterior part of the shaft flares posteriorly at the point of break of the fossil. Just medial to the tibial tuberosity is a hollow depression, posterior to which is a rugose area of bone for the pes anserinus (the common tendon for m. sartorius, m. gracilis, and m. semitendinosus). Laterally, the bone is quite flat and distally the interosseous crest forms and progresses down the length of the shaft becoming most rugose distally. Near the midshaft, there is a concavity between the interosseous crest and the anterior part of the bone for the attachment of m. tibialis anterior. Medially, the bone is relatively flat along its length. On the medial side of the bone there is a border running from superoanteriorly to inferoposteriorly, marking a large attachment of m. flexor digitorum longus. The proximal attachment of m. tibialis posterior is more posteriorly positioned than is typical in modern humans. Posteriorly, the bone is convex and flattens distally. Progressing superolaterally to inferomedially across the proximal part of the posterior shaft is a soleal line. Just medial to the soleal line is a nutrient foramen. On most human tibiae (and on other Dinaledi hominin tibiae), the foramen is lateral to the soleal line. The distal tibia is heavily eroded. Only a small patch of thin subchondral bone is preserved in the tibial plafond, which otherwise has exposed trabeculae. Although the tibiotalar surface is damaged, in lateral view the posterior rim of the tibial plafond is more distally projecting than the anterior rim.

In U.W. 101-484, the dimension of T1–T6 (after Wright and Vásquez, 2003) is 293 mm, resulting in an estimated total tibial length of 325.5 mm (SEE 5.92 mm). Given that nearly the same value was obtained with the comparative and mathematical methods, we estimate that the length of the tibia U.W. 101-484 is approximately 325 mm.

U.W. 101-498 (Fig. 13) is a fragmentary and very gracile (likely immature) left tibial shaft. It does not preserve the tibial tuberosity and the soleal line is barely detectable posteriorly. Just distal to the nutrient foramen, near the distal extent of the soleal line, the bone is 19.8 mm AP and 14.2 mm ML.
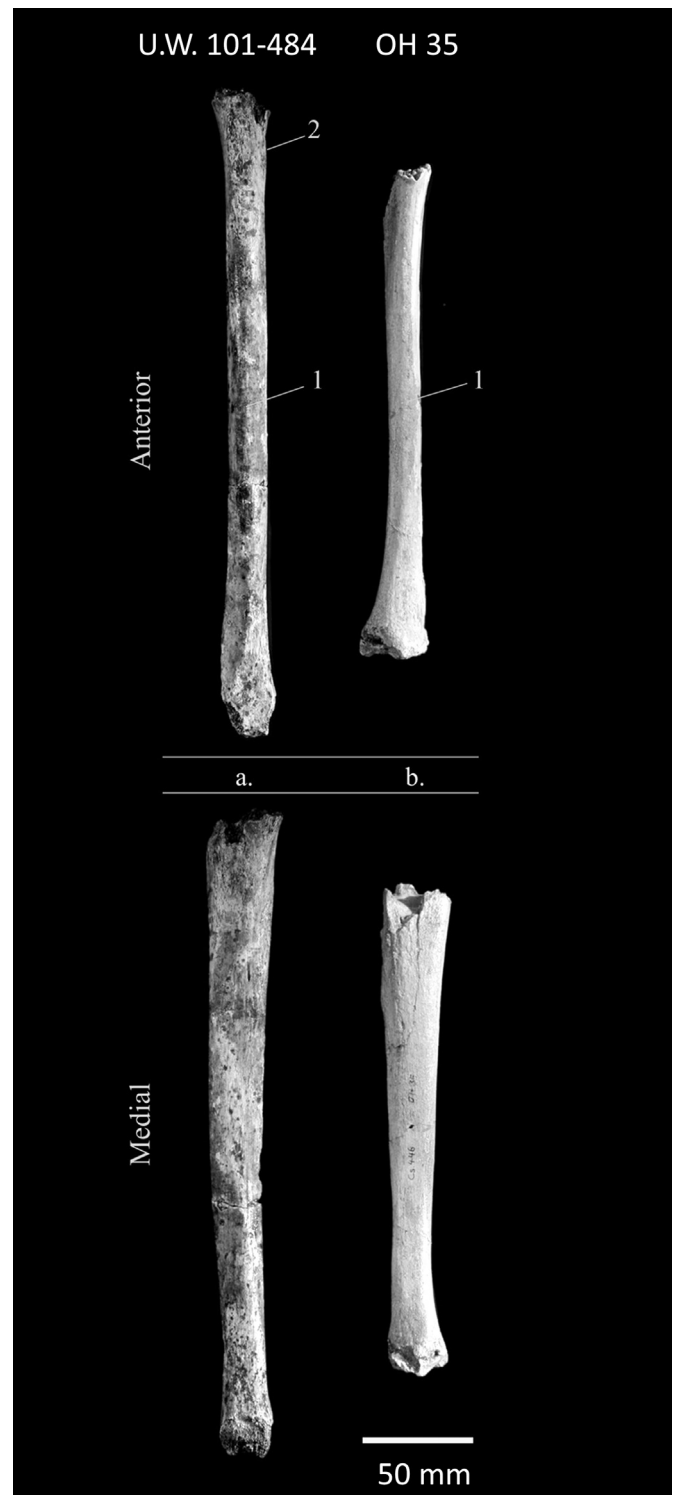

Figure 15. Anterior and medial view of the tibia of (a) *Homo naledi* (U.W. 101-484) and (b) OH 35. Note the straight diaphysis of *H. naledi* as compared to OH 35 in anterior view. *Homo naledi* is also characterized by a relatively less robust tibia due to its longer diaphysis compared to OH 35 (see text). Note the rounded anterior border (1) of U.W. 101-484, similar to OH 35, and proximally the presence of a tubercle for the pes anserinus (2).

U.W. 101-500 (Fig. 13) is a large left proximal tibial shaft. It is broken just distal to the tibial tuberosity, though there are no preserved vertical striations anteriorly and thus it is broken more

distally than U.W. 101-484. Only 94.6 mm SI on the anterior part of the shaft is preserved; the majority of preserved bone is posterior. Laterally, there is a well-developed superoanteriorly to inferoposteriorly directed interosseous crest that progresses down the shaft. Between the anterior border and interosseous crest is a concavity that runs the length of the preserved shaft for m. tibialis anterior. Posteriorly, the distal extent of the soleal line is preserved and elevated, progressing superolaterally to inferomedially. Medially, the bone is convex—flattening anteriorly, with a slight concavity down the length of the shaft posteriorly. Aligning the bones by the soleal line and the interosseous crest, the U.W. 101-500 shaft is 32.2 mm AP and 20.5 ML just distal to the tibial tuberosity, making it roughly the same size as that of U.W. 101-484.

U.W. 101-571 (Fig. 13) is a right proximal tibial shaft. The proximal plateau is sheared away, leaving only the vaguest impression of the inferior vertical striations of the tibial tuberosity. Posteriorly, the bone is damaged, leaving only 50.3 mm SI of the distal portion of the preserved shaft. Laterally, there is a superoanterior to inferoposteriorly running interosseous crest, anterior to which is a depression for the origin of m. tibialis anterior. Medially and most proximally, there is a preserved depression just medial to the tibial tuberosity (which is sheared away) posterior to which there is a rugose area for the pes anserinus (the common insertion of mm. sartorius, gracilis, and semitendinosus). Distally, the medial shaft is quite flat. The shaft is 23.2 mm AP and 17.1 mm ML at the distal break.

U.W. 101-711 (Fig. 14) is a fragmentary mature left distal tibia, preserved from the margins of the tibial plafond to a diagonal break in the tibial shaft. The malleolus has been sheared away, damaging the medial side of the bone. There is erosion around the distal rim of the bone, except for a small patch anteriorly where there is a large squatting facet 4.2 mm SI and a minimum of 7.3 mm ML. The distal metaphysis is AP flared. The talar articular surface is concave AP and mildly concave ML. Medially, there is weak AP keeling. The preserved anterior shaft is flat and there is (eroded) evidence for a large anterior tubercle for the anterior tibiofibular ligament. Medially, the shaft is flat, though there is a palpable pillar separating the anterior and medial portions of the shaft. Posteriorly, the shaft is convex and distolaterally there is a large (eroded) posterior tubercle for the posterior tibiofibular ligament. Laterally, there is a strong interosseous crest descending anterodistally. There is no detectable posterior crest. If there was a fibular facet, it is not preserved at all. In lateral view, the posterior rim of the tibial plafond is more distally projecting than the anterior rim.

U.W. 101-973 (Fig. 13) is a left tibial shaft preserved from a break just distal to the tibial tuberosity to the midshaft area. Just inferior to the tibial tuberosity, the shaft is 32.6 mm AP and 19.3 mm ML, similar to the dimensions of U.W. 101-484 and U.W. 101-500. Just medial to the tibial tuberosity, there is a small hollow depression and, posterior to it, appears to be a raised area for the pes anserinus tendon, though there is considerable damage in this area. Laterally, there is an interosseous crest that begins anteriorly and progresses posteriorly down the shaft. A depression between the anterior crest and the interosseous crest for the m. tibialis anterior runs the length of the shaft. Just posterior to the interosseous crest (laterally) is a nutrient foramen. Posteriorly, there is a well-marked and elevated soleal line running superolaterally to inferomedially.

U.W. 101-996 (Fig. 16) is an immature right tibia, preserved from the proximal metaphyseal surface to the distal metaphyseal
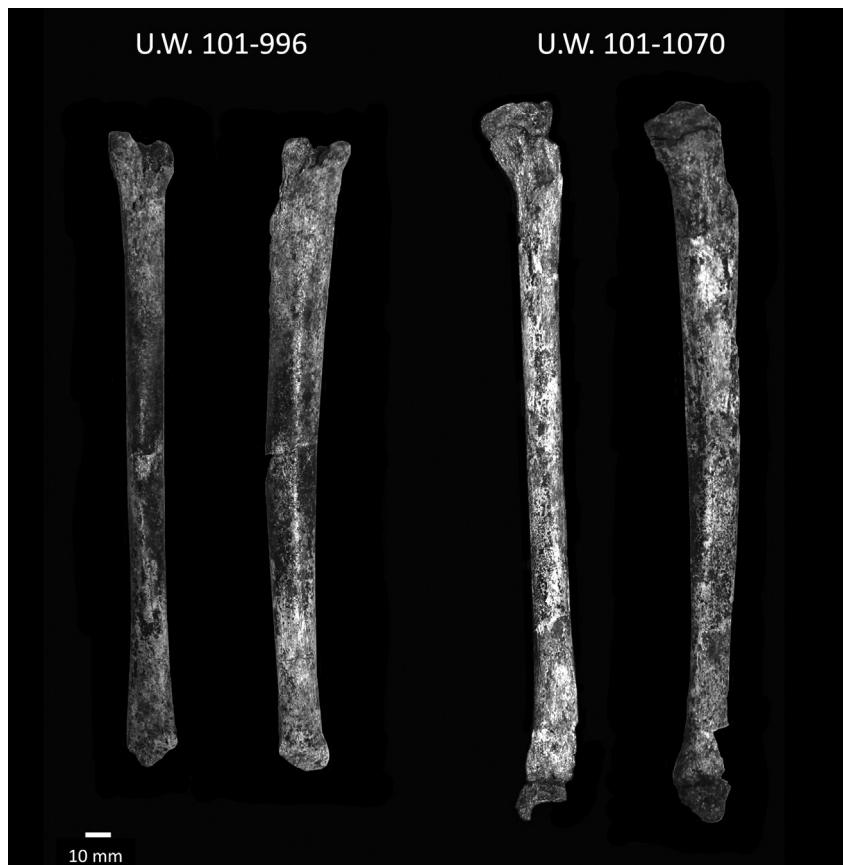

Figure 16. Immature tibiae of *Homo naledi*: U.W. 101-996 and U.W. 101-1070 shown in anterior (left) and medial (right) views. U.W. 101-1070 is the most complete bone from the thigh and leg in the Dinaledi collection. The two fossils are also the only clear antimeres in the thigh and leg assemblage.

surface. It is constituted by three fragments: U.W. 101-996, U.W. 101-1074, and U.W. 101-1077. Only the preservation of this specimen will be described; for anatomical descriptions, refer to the more complete antimere U.W. 101-1070 unless specified otherwise. The three conjoining pieces are (in length): 124.5 mm proximally, 83.7 mm middle, and 45.9 mm distally. The shaft of this specimen is better preserved than U.W. 101-1070. The proximal metaphysis preserves a small patch (9.0 mm ML, 8.5 mm AP) of surface anterolaterally. It is damaged anteriorly and medially, exposing trabecular bone and the medullary cavity. The proximal shaft flares medially and is much straighter laterally. Distally, there is a very small patch of metaphyseal surface (2.8 mm ML, 4.3 mm AP) surrounded by trabecular bone.

U.W. 101-1070 (Fig. 16) is a nearly complete immature left tibia from the tip of the tibial spines to the distal extent of the medial malleolus. Both partially preserved epiphyses were discovered in situ, in articulation on the diaphysis, and are presently (non-permanently) adhered to the shaft. The specimen is well-preserved overall, though there is some damage near the metaphyseal/epiphyseal junctions. The proximal metaphysis is damaged anteriorly and laterally, removing ~16 mm SI of the bone. The lateral condyle is not preserved, but the medial condyle and the tibial spines are present and well-preserved. The distal metaphysis is damaged anteriorly and laterally, such that an 18 mm SI portion of the metaphysis is stripped away anteriorly and anterolaterally, exposing trabecular bone. The medial portion of the medial malleolus is not preserved. The shaft is broken in two locations, producing three parts of the bone: a proximal piece 70.4 mm SI, a middle piece ~144 mm SI, and a distal piece ~78 mm SI (the sum of which exceeds total length because the diagonal breaks and lengths are maximums). The proximal epiphyseal plateau is 29.0 mm AP and a minimum of 28.0 mm ML from the medial edge of the surface to a break at the medial edge of the lateral epicondyle. It is 16.1 mm SI from the tip of the tibial spines to the inferior projection of the tibial tuberosity. The medial epicondyle is moderately concave and measures 23.9 mm AP and 15.5 mm ML. The tibial spines are raised 2.3 mm above the tibial plateau and are 6.7 mm ML apart. They are angled anterolaterally to posteromedially. Anteriorly, there is a small indentation for insertion of the anterior cruciate ligament. The pit for the posterior cruciate ligament is much better developed and is fenestrated with some vascular foramina. The tibial tuberosity is not well-preserved, especially superiorly. Inferiorly, there are vertical striations and in medial view, the base of the tibial tuberosity extends anteriorly. Here the shaft dimensions are 24.9 mm AP and 16.0 mm ML. In medial/lateral view, the tibial plateau exhibits retroversion of 15°. Laterally, a faint interosseous crest begins proximally and continues posterodistally down the shaft. Just anterior to the crest is a weak depression proximally for the m. tibialis anterior. Lateral to the crest, 75.3 mm from the tibial spines is a nutrient foramen. The anterior shaft is strongly convex and the medial surface is relatively flat, especially distally. Posteriorly, the shaft is strongly convex with a bar of bone running distally before flattening near the distal end. The distal end of the tibia is damaged laterally and anteriorly. In medial or lateral view, the posterior part of the bone flares. The AP dimension of the metaphysis is unknown due to damage. There is no preserved fibular facet. The distal epiphysis preserves 18.6 mm ML and 20.5 mm AP. The dimensions of the talar articular surface are not preserved laterally. The ML dimensions cannot be taken, nor can the lateral AP dimensions. The lateral side of the medial malleolus is quite flat. There is a weakly developed intercollicular groove posteriorly for the deltoid ligament and there is some minor erosion medially. Posteriorly, a 3.5 mm ML groove for the m. tibialis posterior tendon runs inferomedially, which is the orientation of the medial malleolus relative to the tibial shaft. The tibial plafond is oriented perpendicular to the long axis of the shaft. In lateral view, the posterior rim of the tibial plafond is more inferiorly projecting than the anterior rim.

U.W. 101-1416 (Fig. 14) is a fragmentary mature right distal tibia, preserved in two conjoining pieces. One is a 44.1 mm SI fragment of a broken shaft and part of the lateral talar facet. The other piece joins distally and is part of the medial talar facet and the medial malleolus. U.W. 101-1416 is associated with the talus U.W. 101-1417, which belongs with the nearly complete foot 1 (Harcourt-Smith et al., 2015). The anteromedial part of the bone has been sheared away, leaving only a small (22.3 mm SI and 14.5 mm ML) patch of cortex anterolaterally. The lateral and posterior parts of the distal shaft are preserved, though the posterior rim is eroded away. The metaphysis flares AP distally. The ML diameter of the metaphysis is unknown due to damage medially. The talar surface is moderately wedged, concave AP, and has a very weak AP keel dividing the facet. The medial malleolus is preserved medially. It is flat, with some convexity anteriorly. Laterally, the medial malleolus is damaged and the cortex is stripped away exposing trabeculae. The medial malleolus is 11.4 mm SI and 7.1 mm ML. The AP dimension is difficult to measure because of damage posteriorly, but is at least 14.1 mm. The preserved shaft has a large laterally positioned anterior tubercle for the anterior tibiofibular ligament. Posteriorly, the shaft is convex and distolaterally there is a large (eroded) posterior tubercle for the posterior tibiofibular ligament. Laterally, there is a strong interosseous crest descending anterodistally and a weak posterior crest. In lateral view, the posterior rim of the tibial plafond is more distally projecting than the anterior rim.

3.4. Fibula

Homo naledi fibula dimensions are listed in Table 6, with material depicted in Figures 17 and 18.

U.W. 101-817 (Fig. 17) is a proximal metaphysis and shaft fragment of an immature left fibula. There is considerable erosional damage leaving only a small portion of the metaphyseal surface of the proximal articulation preserved (11.3 mm AP, 7.5 mm ML, 26.5 mm in circumference). Part of the styloid process is preserved, but proximally and posteriorly there is erosional damage. The proximal articular surface is angled proximolaterally to distomedially (125° to the longitudinal axis of the bone). The preserved shaft is ML compressed (10.3 mm AP, 6.2 mm ML). The anterolateral and posterolateral borders are visible, but poorly defined. The anteromedial border is not visible. The posteromedial border is well-marked. The presence of a broken portion medially and many cracks potentially contribute to the less triangular appearance in cross-section of the shaft compared to the fragmentary specimens U.W. 101-1113 and U.W. 101-1451.

U.W. 101-1037 (Fig. 18) is a left fibular diaphyseal shaft (roughly four-fifths complete) constituted by two conjoining fragments, U.W. 101-1037 and U.W. 101-1498. The proximal end nears the level of the neck as suggested by the constriction of the diaphysis and the triangular cross-sectional shape. The flaring that occurs in fibulae just distal to the head is not observable in this specimen. The distal break presents trabecular bone indicating the break is near the malleolus. Distally, in posterior and anterior view, flaring characteristic of the origin of the malleolus is evident. The anterolateral border starts proximally, is well-marked and sharp, and becomes blunter distally. The border bifurcates 26.5 mm from the distal break, marking the beginning of the subcutaneous triangular surface (STS). Only a small portion of the STS is present. The lateral border of the STS is sharp and slightly convex posteriorly. The anteromedial border is not visible proximally. A distance of 29 mm distal to the proximal break, the anteromedial border is visible and runs parallel to the anterolateral border for ~50 mm. The

Table 6
Comparative fibula dimensions.[a]

Specimen/Species	Neck ML	Neck AP	Neck robusticity (ML/AP) × 100[b,c]	Midshaft ML	Midshaft AP	Midshaft robusticity (ML/AP) × 100	Angle between STS and fibulotalar surface[d]	Area of proximal portion fibulotalar articulation	Area of distal portion fibulotalar articulation
U.W. 101-702	7.5	7.7	97.4	–	–	–	–	–	–
U.W. 101-925	5.3	7.3	72.6	–	–	–	–	–	–
U.W. 101-1037	7.0	7.2	97.4	8.1	9.8	82.2	–	–	–
U.W. 101-1113	6.9	7.1	97.2	–	–	–	–	–	–
U.W. 101-1143	7.8	8.2	95.1	–	–	–	–	–	–
U.W. 101-1254	8.0	10.2	78.4	–	–	–	–	–	–
U.W. 101-1437	–	–	–	–	–	–	36	113.6	43.6
U.W. 101-1451	6.9	7.0	98.6	–	–	–	–	–	–
U.W. 101-1679	7.6	8.4	86.0	–	–	–	–	–	–
U.W. 101-1701	–	–	–	–	–	–	–	–	41.3
Homo naledi[e]	7.1 ± 0.9 5.3–8.0 ($n = 8$)	7.9 ± 1.1 7.0–10.2 ($n = 8$)	89.9 ± 10.3 72.6–98.6 ($n = 8$)	8.1 ($n = 1$)	9.8 ($n = 1$)	82.2 ($n = 1$)	36.0 ($n = 1$)	113.6 ($n = 1$)	42.5 41.3–43.6 ($n = 2$)
Gorilla gorilla	12.9 ± 2.5 9.3–16.0 ($n = 7$)	17.0 ± 2.4 12.5–19.6 ($n = 7$)	75.8 ± 8.2 65.6–88.1 ($n = 7$)	12.4 ± 1.3 9.9–13.6 ($n = 7$)	15.5 ± 2.3 12.1–17.9 ($n = 7$)	80.8 ± 8.6 68.9–94.5 ($n = 7$)	57.1 ± 7.7 42.6–70.2 ($n = 11$)	279.6 ± 76.3 169.7–451.6 ($n = 27$)	97.2 ± 35.9 46.1–177.7 ($n = 27$)
Pan troglodytes	8.6 ± 2.5 4.6–12.5 ($n = 10$)	12.2 ± 2.4 6.8–15.2 ($n = 10$)	71.8 ± 22.3 37.9–108.7 ($n = 10$)	9.6 ± 1.5 6.8–11.9 ($n = 10$)	13.0 ± 2.3 7.4–15.3 ($n = 10$)	74.9 ± 10.0 58.1–92.6 ($n = 10$)	49.3 ± 9.1 29.4–65.6 ($n = 17$)	154.0 ± 34.1 88.4–236.0 ($n = 29$)	45.5 ± 16.5 12.6–88.2 ($n = 29$)
Homo sapiens	9.4 ± 1.7 6.6–12.4 ($n = 23$)	11.6 ± 1.6 7.5–13.8 ($n = 23$)	81.8 ± 16.6 52.6–111.5 ($n = 23$)	11.5 ± 2.0 8.6–15.0 ($n = 23$)	14.8 ± 1.9 11.4–19.1 ($n = 23$)	78.5 ± 12.5 61.1–102.0 ($n = 23$)	34.2 ± 4.8 25.0–46.0 ($n = 28$)	162.6 ± 32.0 113.1–257.0 ($n = 34$)	63.5 ± 21.5 14.9–103.1 ($n = = 34$)
Australopithecus sp.[f]	9.2 ± 1.6 8.4–10.0 ($n = 2$)	9.8 ± 2.6 8.0–11.6 ($n = 2$)	95.7 86.3–105.0 ($n = 2$)	11.9 ($n = 1$)	11.1 ($n = 1$)	106.9 ($n = 1$)	37.6 ± 3.4 34.0–42.0 ($n = 5$)	141.5 ± 18.4 111.0–159.6 ($n = 5$)	21.0 ± 11.2 3.7–33.7 ($n = 5$)
Early *Homo*[g]	9.1 ($n = 1$)	8.2 ($n = 1$)	111.1 ($n = 1$)	11.0 ($n = 1$)	11.8 ($n = 1$)	93.4 ($n = 1$)	–	–	–
Homo erectus[h]	5.9 ± 0.4 5.6–6.1 ($n = 2$)	10.0 ± 0.1 9.9–10.1 ($n = 2$)	58.5 ± 2.7 56.6–60.4 ($n = 2$)	9.0 ± 0.1 8.9–9.1 ($n = 2$)	11.5 ± 1.4 10.5–12.5 ($n = 2$)	78.9 ± 10.9 71.2–86.7 ($n = 2$)	–	–	–

[a] Measurements taken on high quality casts or original specimens unless noted otherwise
[b] ML = mediolateral breadth of the fibular shaft at the neck, AP = anteroposterior breadth of the fibular shaft at the neck
[c] Linear measurements are in mm, areas in mm², angular measurements are in degrees. Measurements are represented by mean ± std.dev., range, and sample size
[d] STS: subcutaneous triangular surface. Angle measured following indications in Marchi (2015)
[e] Mature specimens: U.W. 101-702, U.W. 101-925, U.W. 101-1037, U.W. 101-1113, U.W. 101-1143, U.W. 101-1254, U.W. 101-1437, U.W. 101-1451, U.W. 101-1679, U.W. 101-1701
[f] A.L. 288-1at, A.L. 333-9a, A.L. 333-9b, A.L. 333-85, A.L. 333-w37, StW 356, U.W. 88-23
[g] OH 35
[h] KNM-WT 15000 (juvenile)

anteromedial border then diverges medially and is no longer visible 49 mm from the distal break, though erosion of the surface may contribute to the loss of this border. The posteromedial border is well-marked and sharp proximally, extending 48 mm from the proximal break. More distally, the posteromedial border remains well-marked, but it is not sharp. Distally, it becomes continuous with the area for interosseous ligament attachment. This area appears grooved and is 23.8 mm SI. The most proximal part of the interosseous ligament insertion is at the same level as the most proximal portion of the STS. The posterolateral border is damaged proximally. More distally, it is well-marked and rounded. The anterior surface is flat for its entire length. It is very narrow (2.6 mm ML) until midshaft and increases in breadth distally. The medial surface is distinctly grooved proximally (proximal insertion of m. tibialis posterior) until about 50 mm from the proximal break. The groove becomes shallower approaching midshaft, where it becomes flat and then slightly convex distally. There is some erosional damage around midshaft and the mid-distal shaft. The lateral surface is grooved proximally until 74 mm from the proximal break. The groove decreases in depth and disappears at midshaft, where the surface becomes convex (for the proximal insertion of m. fibularis brevis). This convexity increases distally. The surface is directed anterolaterally on the proximal portion, then spirals and is directed laterally on the distal portion. A section of cortex is missing around midshaft on the lateral surface. The posterior surface is slightly grooved proximally until ~45 mm from the proximal break.

Distally it is flat for the majority of the diaphysis. It becomes convex 63 mm from the distal break and becomes more convex distally. At the distal break, the dimensions are 11.8 mm AP, 8.3 mm ML, and 31.7 mm in circumference.

The fibula neck-STS distance in U.W. 101-1037 is 207 mm. Therefore, the complete length of U.W. 101-1037 is estimated to be 328.1 mm. This estimation is based on the assumption that the insertion for the STS is human-like, being more proximal than in apes. Only two other early hominin fibulae are complete enough to use for reference, StW 356 and OH 35. StW 356 does not include the distal articular surface, so the most proximal portion of the STS cannot be established with confidence. In OH 35, the proximal portion of the STS is quite distal, far more so than in modern humans. Using the same regression formula used for *H. naledi*, the estimated length of the fibula for OH 35 (neck-STS = 155 mm) is 261.5 mm, almost identical to the 259 mm estimated by Susman and Stern (1982). Using a regression calibrated on apes (which have shorter proximal portions of the STS than humans: fibula length (mm) = −19.57 + 1.673 × neck-STS, R² = 0.70; N = 30; SEE = 8.8) produces an even shorter fibula length for OH 35 (fibula length = 239.7 mm). Therefore, we are confident the regression equation calibrated on humans is appropriate to estimate fibular length in *H. naledi*.

U.W. 101-1045 is an immature left fibula consisting of three non-conjoining fragments. The proximal fragment (length 19.7 mm) is badly damaged, with only a portion of the metaphyseal plate and some cortex visible. The metaphyseal surface is rectangular (9.0 mm
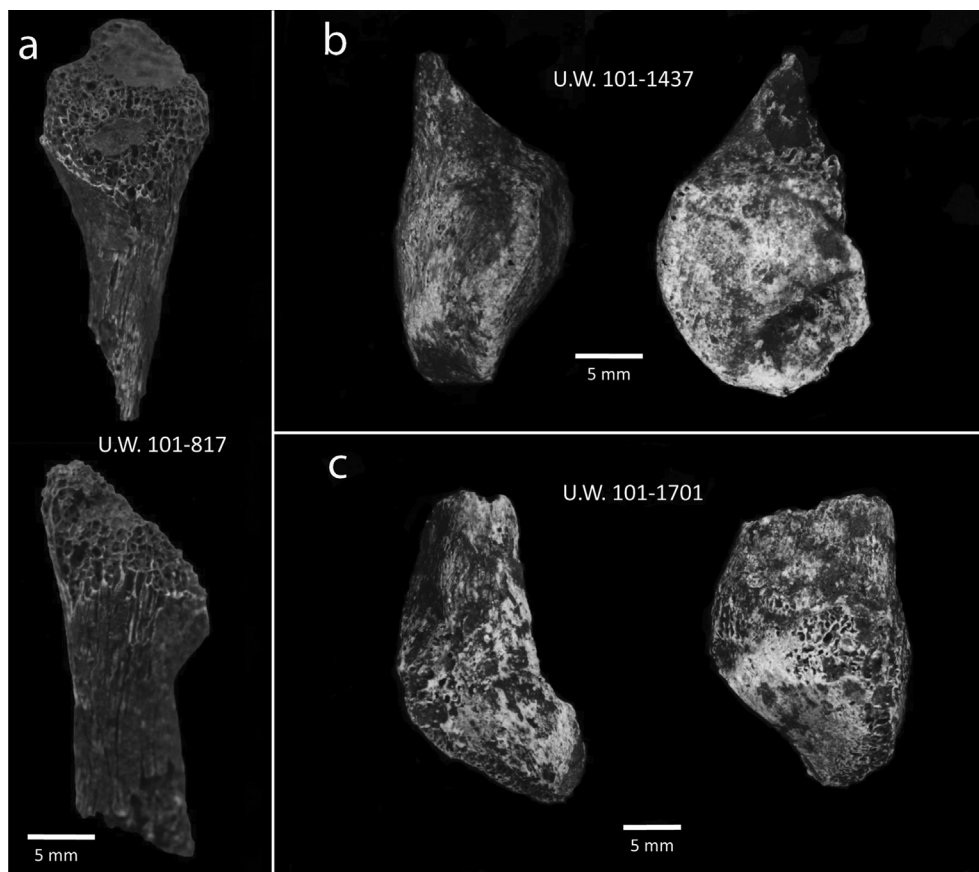
Figure 17. Fibular epiphyses of *Homo naledi*. (a) Medial view (top) and anterior view (bottom) of the immature U.W. 101-817 left proximal fibula, (b) anterior view (left) and medial view (right) of the mature U.W. 101-1437 right distal fibula, (c) anterior view (left) and medial view (right) of the mature U.W. 101-1701 left distal fibula.

AP, 8.8 mm ML). A second proximal fragment (length 75.9 mm) is platycnemic in cross-section proximally and triangular distally. The proximal break is jagged and the distal break is sheared cleanly. The diameters at the distal break are 8.6 mm AP and 7.1 mm ML. The lateral and posterior surfaces are eroded proximally. Some damage is present on the medial surface. The more distal fragment (length 112.2 mm) is probably distal midshaft. There is damage to the posteromedial border and some erosion on the lateral surface. The proximal break of the distal fragment is jagged and its diameters are 8.3 mm AP and 7.2 mm ML. The distal break is jagged. The antero-lateral border is well-marked along the entire shaft. It is sharp proximally and gradually becomes more rounded distally. Distally, the bone is broken before the anterolateral border bifurcates to form the subcutaneous triangular surface. The anteromedial border is not visible. The posteromedial border is well-defined and moderately sharp proximally. It becomes more rounded distally. The postero-lateral border is directed posteriorly and slightly laterally along its entire length. The medial surface is deeply grooved proximally, slightly convex around midshaft, and flat distally. Some erosion on the mid-distal portion makes it difficult to precisely define the appearance of the surface. The lateral surface of the bone is eroded proximally. It is flat from proximal to midshaft and slightly convex from midshaft distally. The posterior surface is flat. Erosion proxi-mally makes it difficult to measure minimum diameter and circumference. The largest diameter of the cross section of the diaphysis changes from AP proximally, to ML at midshaft, to AP again distally. The diameter at the level of the proximal break of the distal fragment is 7.6 mm AP and 7.5 mm ML.

U.W. 101-1437 (Fig. 17) is a mature right distal fibula from the most distal part of the lateral malleolus to the proximal break. Only a small portion of the STS is preserved. The posterior part of the malleolus has been stripped away. The distal tibiofibular articula-tion is preserved: it is small, crescent-shaped, and oriented supe-riorly. The talofibular articulation is almost completely preserved. The proximal portion of the talofibular articulation is rectangular and a small part is missing posteriorly. The distal part of the talo-fibular articulation is preserved and triangular in shape. The mal-leolar fossa on the medial side of the articulation is deep, elongated anterosuperiorly to posteroinferiorly, and contains vascular foramina.

U.W. 101-1701 (Fig. 17) is a mature left distal fibula fragment, preserved from the most distal part of the lateral malleolus to the proximal break. The lateral side of the malleolus and part of the anterior side have been stripped away. Medially, the distal portion of the interosseous ligament insertion area is preserved (15.6 mm SI) and the area is grooved. The AP diameter, superior to the fibulotalar articulation, is 17.2 mm. The distal tibiofibular articulation on the medial aspect is small, eroded, and oriented superiorly. The superior part of the proximal part of fibulotalar articulation is eroded. The distal part of the fibulotalar articu-lation is preserved and triangular in shape. Only the anterior border of the malleolar fossa is preserved medially. The poste-rior portion of the malleolar fossa has been stripped away. The preserved malleolar fossa is deep and elongated ante-rosuperiorly to posteroinferiorly. Some vascular foramina are visible.
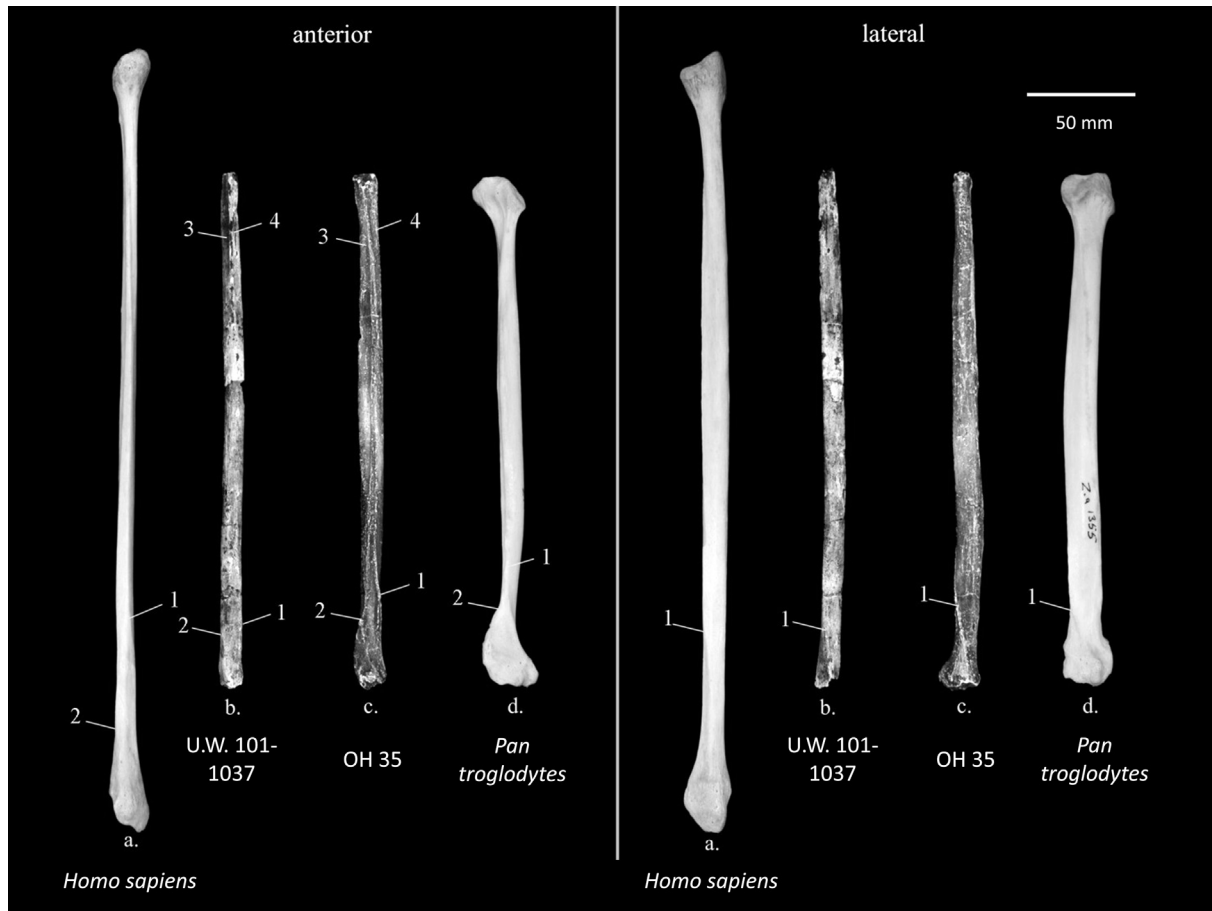
Figure 18. (a) Modern human fibula compared to (b) *Homo naledi* (U.W. 101-1037), (c) OH 35, and (d) *Pan troglodytes*. Note the proximal portion of the subcutaneous triangular surface (STS; 1) and of the interosseous ligament insertion (ILI; 2). In U.W. 101-1037, the proximal portion of the two structures is more or less at the same level in the diaphysis, similar to OH 35 fibula. In humans, the STS is more cranial than the ILI. Note the grooves for m. tibialis posterior (3) and m. peroneus longus (4) in U.W. 101-1037, also present in the OH 35 fibula.

4. Comparative anatomy (results and discussion)

4.1. Femur

The femur of *H. naledi* is represented by 26 proximal and diaphyseal elements, and three fragments of the distal femur, attributed to a minimum of eight mature and three immature individuals (Table 2). Table 3 lists *H. naledi* femoral dimensions compared to fossil hominins, extant humans, and apes. In the DFA, (Fig. 19a) modern human femora are separated from hominin indet. along function 1, which accounts for the majority (87.7%) of the variance. Grouped with the hominin indet. specimens are KNM-ER 1503 and OH 20, femora generally attributed to eastern African robust australopiths (Day, 1969; McHenry and Corruccini, 1978). The variables driving function 1 are neck length (longer to the right) and neck breadth (narrower to the left). Thus, the long, anteroposteriorly compressed necks of the eastern African robust australopiths cluster to the right. Fossils attributed to *Homo* align with modern humans along the first discriminant function, but fall below modern humans along function 2, which is being driven by neck SI diameter in the positive direction and neck length in the negative direction. Subtrochanteric AP is the only variable that does not make a significant contribution ($p = 0.45$) to the discriminant functions. Fossils of *A. afarensis*, *A. africanus*, *A. robustus*, *A. sediba*, and *Homo floresiensis* occupy the morphospace between modern humans, early *Homo*, and those presumed to belong to *A. boisei*. The Dinaledi femora span the gap between early *Homo* and *Australopithecus* with two femora (U.W. 101-002 and U.W. 101-398) clustering with the australopiths and one femur (U.W. 101-1391) clustering with early *Homo*.

Because group membership is assumed a priori in DFA, we reran the analysis without the hominin indet. femora and found similar results to the initial DFA (Fig. 19c). Again, the *H. naledi* femora cluster between femora attributed to fossil *Homo* and those attributed to *Australopithecus*. Group membership was predicted to be *Australopithecus* for U.W. 101-002 and fossil *Homo* for U.W. 101-398 and U.W. 101-1391, indicating the morphological mosaic of the Dinaledi femora.

Homo naledi femora possess a combination of traits found in both australopiths and early *Homo* (Tables 7 and 8). The femoral neck is relatively long, consistent with the flaring of the preserved ilium from the Dinaledi chamber (Berger et al., 2015; Van Sickle et al., in this issue). Relative to the subtrochanteric dimensions (square root of the product of the AP and ML diameters), the femoral neck is long in australopiths and in early *Homo* (Fig. 20), with *H. naledi* femora falling within the overlapping ranges. However, the femoral necks are SI tall and AP compressed (Table 3), more similar to the morphology found in australopiths (Ruff and Higgins, 2013) and quite distinct from the femoral neck shape in specimens attributed to *Homo* (Fig. 21; Ward et al., 2015). The subtrochanteric region of the shaft is platymeric (Fig. 22), though not as platymeric as is typically found in *H. erectus*. However, this
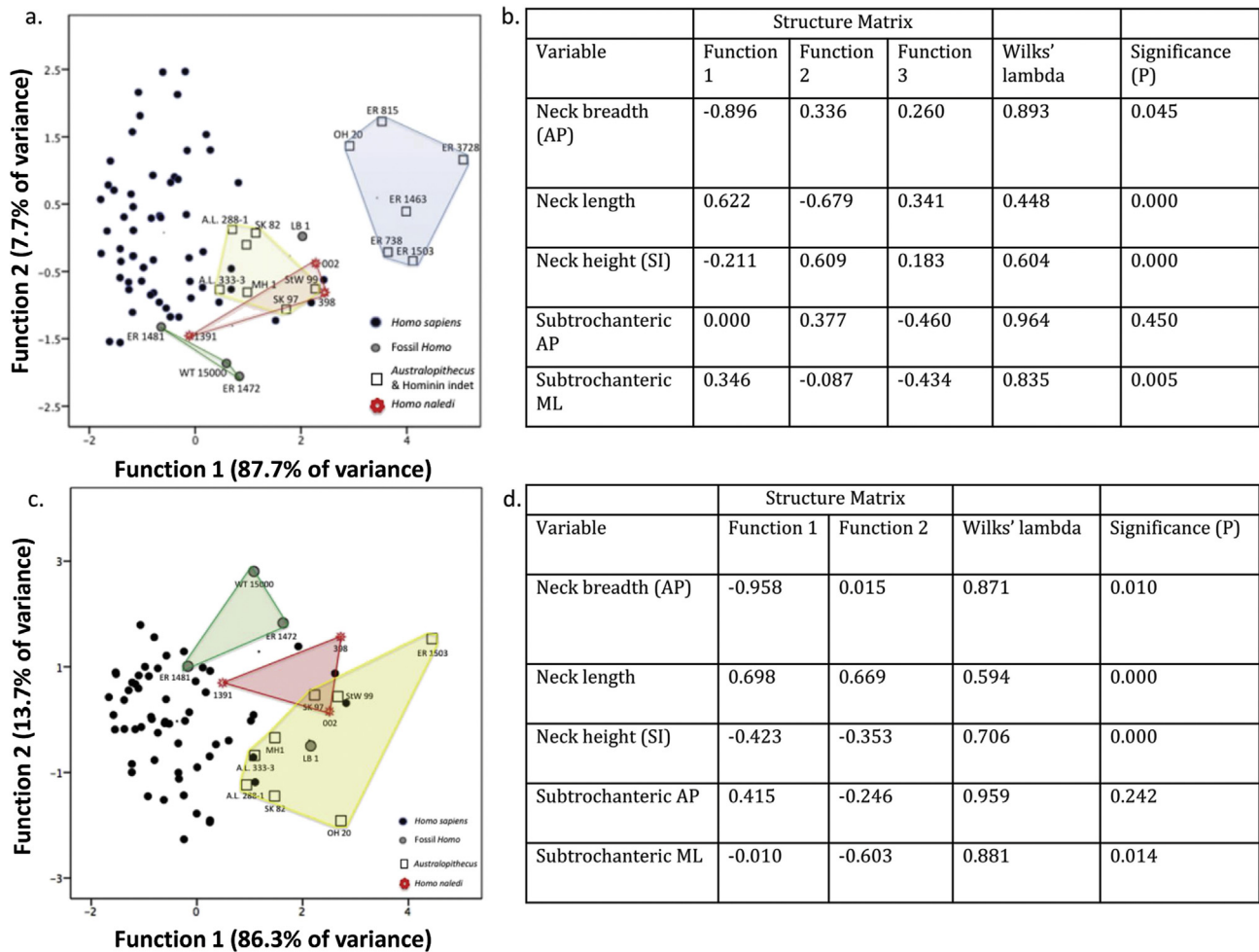
Figure 19. (a) Discriminant function analysis (DFA) of proximal femoral shape among hominins. The Dinaledi femora (shaded in red) span the gap between fossils attributed to *Australopithecus* (shaded in yellow) and early *Homo*, including *H. erectus* (shaded in green). To the right (shaded in blue) are fossils generally attributed to *A. boisei* (OH 20 and KNM-ER 1503) clustering with many fossils only identified as "hominin indet.," suggesting that these too may belong to *A. boisei*. (b) DFA structure matrix based on shape variables, along with Wilks' lambda and significance values. (c) DFA of proximal femoral shape among hominins as presented in [a] except that the uncertain "Hominin indet." specimens were not included. Again, the Dinaledi femora (shaded in red) plot in the space between fossil *Homo* (shaded in green) and *Australopithecus* (shaded in yellow). (d) DFA structure matrix based on shape variables, along with Wilks' lambda and significance values. Measurements are defined in the text. (For interpretation of the references to color in this figure legend, the reader is referred to the web version of this article.)

difference does not reach statistical significance (Student's *t*-test; $p = 0.13$) with the current sample sizes. While the femoral shaft of *H. erectus* remains mediolaterally expanded at midshaft, the Dinaledi femora all become AP expanded inferior to the platymeric subtrochanteric region and remain AP expanded throughout the length of the shaft (see description of U.W. 101-012, for example). This shaft anatomy contrasts sharply with that found in *H. erectus* and is more similar to earlier *Homo* specimens, which are AP expanded at midshaft (Ward et al., 2015). The Dinaledi femora are characterized (especially in larger individuals, Fig. 4f) by considerable femoral anteversion, which contributes to an anterior set of the femoral neck relative to the proximal shaft (Fig. 4, medial views), as is found in australopiths and in early *Homo* (Fig. 23). While modern human femora exhibit a wide range of femoral neck anteversion, the neck is typically not torqued relative to the proximal shaft (Fig. 1c) and overall femoral neck anteversion is instead a reflection of the morphology of the distal diaphysis (Kingsley and Olmsted, 1948; Aiello and Dean, 2002). Other traits in the proximal femur that have been purported to distinguish *Homo* from australopiths, such as a lesser trochanter that is visible in anterior view (Pickford et al., 2002) or a sustrochlear hollow (Tardieu, 2010),

are variably present in both *Homo* and *Australopithecus*, as well as in *H. naledi*. As with other hominin femora, the distribution of cortical bone in the femoral neck is asymmetrical (Ohman et al., 1997), there is a carrying angle at the knee, and the lateral condyle is flat and elongated (Lovejoy, 2007). Together, these anatomies are consistent with a hominin that practiced full extension of the leg during a human-like, striding bipedal gait.

Homo-like traits in the proximal diaphysis of the *H. naledi* femur include a well-defined posteriorly positioned gluteal tuberosity, a well-developed linea aspera, a variably present pilaster (see Fig. 10), and a thick diaphyseal cortex (Table 3; Figs. 4–6, 9). As in *H. erectus* femora (Gilbert, 2008), the cortex is thicker medially than laterally on all femoral shafts. Though while thick cortex is generally thought to characterize the femora of early *Homo* (Gilbert, 2008), the femoral shaft of a recently described *A. boisei* skeleton, OH 80, also has thickened cortex (Domínguez-Rodrigo et al., 2013). In the Dinaledi femora, the base of the greater trochanter appears to flare laterally, as it does in other *Homo* femora. However, this observation remains qualitative and suffers from a lack of fully preserved greater trochanters on any of the Dinaledi femora. The immature femur U.W. 101-938 possesses an inferolaterally angled

ARTICLE IN PRESS

Table 7
Phenetic comparisons of postcranial morphology in *Australopithecus* and early *Homo*.[a]

	A. afarensis[b]	*A. africanus*[c]	*A. sediba*[d]	*H. habilis*[e]	*H. naledi*	*Homo* sp.[f]	*H. erectus*[g]
Femur							
Neck cross-sectional long axis	Superoinferior oriented	Superoinferior oriented	Anterosuperior to Posteroinferior oriented	Superoinferior oriented	Anterosuperior to posteroinferior oriented	Moderately anterosuperior to posteroinferior oriented	Moderately anterosuperior to posteroinferior oriented
Lateral expansion of greater trochanter	Weak	Weak	—	—	Present	Strong	Stong
Proximal diaphyseal cross-sectional shape	Mediolaterally expanded but not buttressed	Strongly mediolateral buttressed	Mediolaterally expanded but not buttressed	Approx. circular	Moderately mediolaterally buttressed	Strongly mediolaterally buttressed	Strongly mediolaterally buttressed
Midshaft-to-mid-proximal (50–65%) %CA	—	(80)	84.4	83.2	87	85.6	65.2–86.8
Pilaster	Variably present	Present	Absent	Present	Present (weak)	Absent	Slight
Linea aspera	Weak	Weak	Weak	Prominent	Prominent	Prominent	Prominent
Patella							
Anteroposterior thickness	—	—	Intermediate	—	Human-like	—	—
Tibia							
Popliteal (soleal) line	Prominent	Prominent	Moderate?	Strongly marked	Strongly marked	Marked?	Marked
Proximal shaft curvature	Slight, convex medially	Absent	Absent	Slight, convex medially	Absent	Absent	Absent
Diaphyseal anterior border	Rounded?	—	Sharp	Rounded	Rounded	Sharp?	Rounded
Distal shaft curvature	Slight (convex laterally) to absent	—	Slight, convex laterally	Slight, convex laterally	Slight, convex laterally	—	Slight, convex laterally
Morphology of triangular attachment area for inferior interosseous ligament	Poorly marked, Superoinf. short	Poorly marked, superoinf. short	Poorly marked, superoinf. short	Well-marked and elongate	Well-marked and elongate	Well-marked and elongate	Poorly marked, elongate
Medial malleolar thickness	Thin	Thin	Thick	Thin	Thin	Thin	Thin
Talar articular surface orientation (as seen in lateral view)	Variably anteriorly or posteriorly tilted	Variably anteriorly tilted or neutral	Anteriorly tilted	Anteriorly tilted	Anteriorly tilted	Neutral (90°)	Anteriorly tilted
Fibula							
Peroneus longus origin shape	—	Convex	—	Convex	Convex	—	—
Distal tibiofibular articular facet	Small and cresentic	—	Rectangular	Small and cresentic	Small and cresentic	Oval	—

[a] The postcranial features described in this table are not intended as an exhaustive list of the morphological attributes of *Homo naledi* postcranial skeletons. Postcranial character states for various taxa were derived from the literature where noted, otherwise data derive from measurements and observations taken by the authors on the original fossil material, or, in the case of specimens from Hadar and Olduvai Gorge, casts (from ref. 7 Berger et al., 2010)

[b] As represented by A.L. 137-48A, A.L. 211-1, A.L. 288-1ap, A.L. 322-1, A.L. 333-3, A.L. 333-4, A.L. 333-6, A.L. 333-7, A.L. 333-9a, A.L. 333-9b, A.L. 333-75, A.L. 333-85, A.L. 333-95, A.L. 333-111, A.L. 333w-37, A.L. 333X-6/9, A.L. 333x-26, A.L. 438-1, MAK-VP 1/1, and MAK- VP 1/3

[c] As represented by MLD 46, Sts 7, Sts 14, StW 25, StW 88, StW 99, StW 102, StW 181, StW 311, StW 347, StW 358, StW 363, StW 389, StW 392, StW 403, StW 431, StW 443, StW 479, StW 486, StW 501, StW 514, StW 522, StW 527, StW 573, and StW 598

[d] As represented by MH1 and MH2

[e] *H. habilis* postcranial hypodigm taken as OH7, OH8, OH35, OH48, OH62, and KNM ER 3735

[f] Postcranial material conventionally considered to represent early *Homo*, but without associated taxonomically-diagnostic craniodental remains: KNM ER 1472, KNM ER 1475, KNM ER 1481, KNM ER 3228, and OH 28

[g] *H. erectus* (*ergaster*) represented by KNM-WT 15000, KNM-ER 803, KNM-ER 1808, KNM-BK 66, BSN49/P27, and postcranial material from Dmanisi possibly associated with the D2600 cranium (D4166, D4161, D4507, D4167, D3901, D4110, D2021, D4165, D4058)

Table 8
Summary thigh and leg morphology of *Homo naledi*.[a]

Traits	Femur and Patella	Tibia	Fibula
Homo-like	- Long neck - Strong insertion of m. gluteus maximus - Well-marked linea aspera - Distal shaft waisting - AP thick patella	- Relatively (to femoral head size) long	- Gracile fibula - Laterally oriented lateral malleoli
Australopith-like	- AP compressed, SI tall and anteverted neck	- ML compressed - Large proximal attachment for m. tibialis posterior	- Circular neck - Convex surface for attachment of m. peroneus brevis
Unique	- Two bony pillars on the superior aspect of the neck	- Strong pes anserinus attachment	

[a] AP = anteroposterior, SI = superoinferior, ML = mediolateral
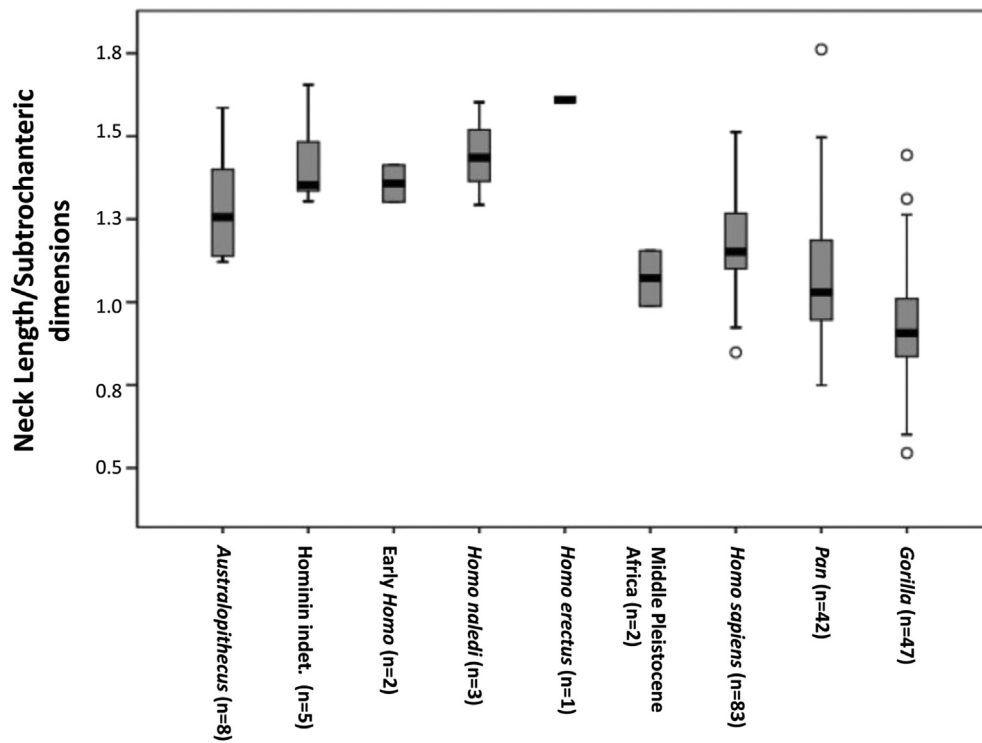
Figure 20. Relative length of the femoral neck in *Homo naledi* compared to fossil hominins and extant humans and apes. The femoral neck length is divided by the square root of the product of the mediolateral and anteroposterior dimensions of the subtrochanteric region of the shaft. The box-and-whisker plots show the median (dark horizontal line), upper and lower quartiles (boxes), range (whiskers), and outliers (circles). The 95% confidence interval of the slope of the RMA regression line characterizing the scaling relationship between neck length and subtrochanteric dimensions includes 1.0 (0.994–1.275), justifying the treatment of these data as a ratio. The lone *H. erectus* fossil is the KNM-WT 15000 juvenile, which may have such a long relative neck because it is an immature individual. Note the position of relative neck length in the Dinaledi femora within the range of *Australopithecus* and early fossil *Homo*.

metaphyseal surface for the greater trochanter, like that found in the *H. erectus* juvenile KNM-WT 15000 and unlike immature australopith femora (Ward et al., 2012). Distal waisting is another femoral character that has been attributed to early *Homo* (Ruff, 1995), and *H. erectus* in particular (Gilbert, 2008; Puymerail et al., 2012). Though there are no complete femora from the Dinaledi chamber, specimen U.W. 101-003 is complete enough to demonstrate that shaft waisting occurs distally (see Fig. 6). U.W. 101-003 gradually decreases in ML diameter distally down the shaft and is at its narrowest where the bone is broken distally and trabecular bone is exposed, indicating proximity to the distal metaphysis.

In our view, there is also a unique feature—consistently present in all *H. naledi* proximal femora—not observed in other hominins: an elongated depression in the superior aspect of the neck that contributes to the presence of two mediolaterally-oriented pillars

of bone, one inferoposterior and the other superoanterior. A depression between these two pillars is highly vascularized. Seen as a sagittal plane section along the neck-shaft boundary, the depression and resulting pillars are pronounced and distinct (Figs. 2 and 5). Subtle hints of this anatomy can be seen in some other hominin femora (e.g., U.W. 88-4 [*A. sediba*], KNM-ER 1472 [early *Homo*]) but none exhibit it to the extent found in all of the Dinaledi femora. While the consistency of this anatomy, among many others, supports our interpretation of the Dinaledi assemblage as a single species (Berger et al., 2015; Dirks et al., 2015), the functional implication of such a femoral architecture remains unknown. They may constitute bony reinforcement to bending forces across the superior neck, perhaps related to the flaring ilia of the pelvis of *H. naledi* (Berger et al., 2015). Their presence may therefore imply different biomechanics of the hip compared with other hominins.
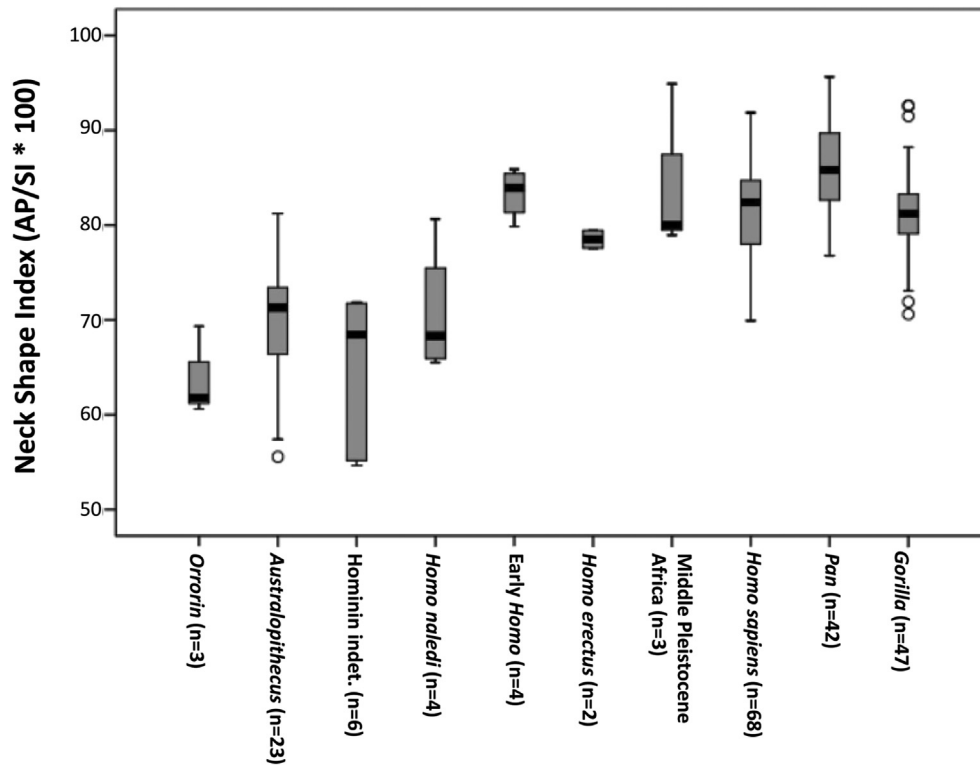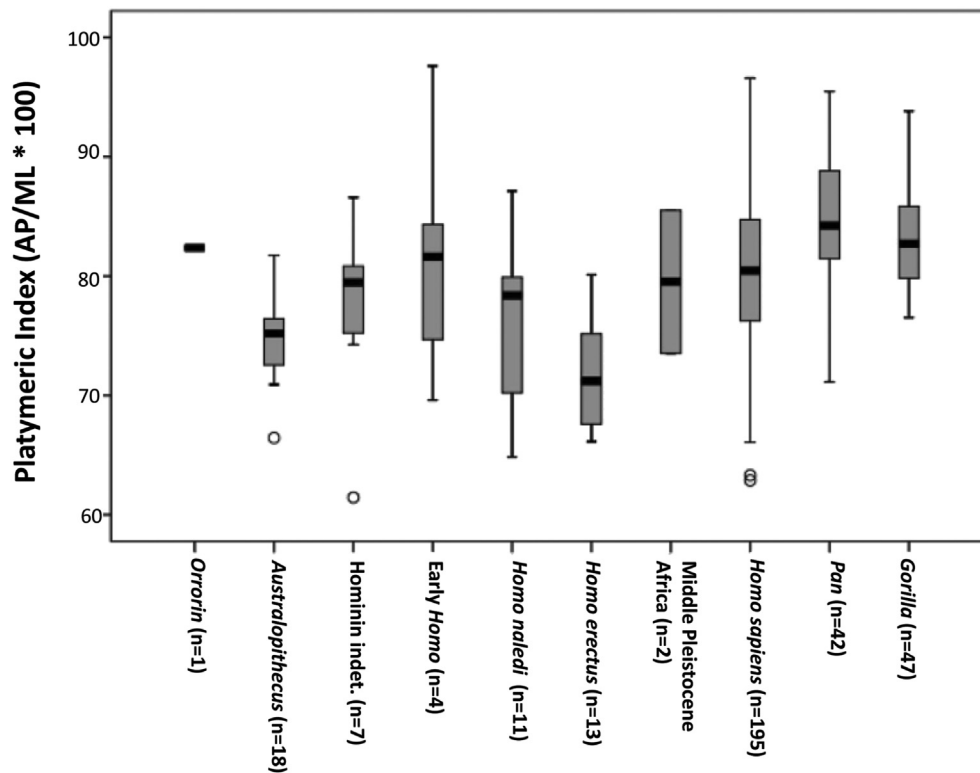
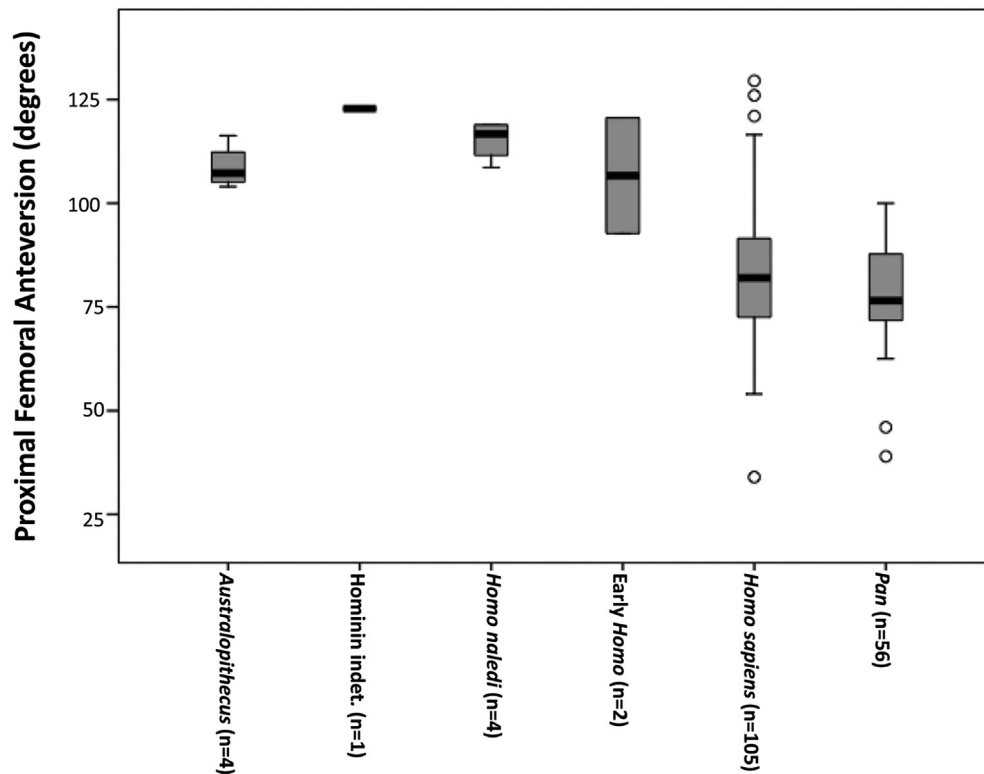**Figure 21.** Relative shape of the femoral neck in *Homo naledi* compared to fossil hominins and extant humans and apes. The box-and-whiskers plots show the median (dark horizontal line), upper and lower quartiles (boxes), range (whiskers), and outliers (circles). Individual values are listed in DeSilva et al. (2013) and Ward et al. (2015). The 95% confidence interval of the slope of the RMA regression line characterizing the scaling relationship between neck SI and ML diameters includes 1.0 (0.911—1.022), justifying the treatment of these data as a ratio. Fossil *Homo* has a more circular femoral neck, whereas the femoral neck of earlier hominins is anteroposteriorly compressed. The Dinaledi femora are australopith-like in having a more compressed neck than fossil *Homo*, though one individual (U.W. 101-1391) is in the range of early *Homo*.

Figure 22. Platymeric index in *Homo naledi* compared to fossil hominins and extant humans and apes. The box-and-whiskers plot shows the median (dark horizontal line), upper and lower quartiles (boxes), range (whiskers), and outliers (circles). Individual values are listed in DeSilva et al. (2013). The 95% confidence interval of the slope of the RMA regression line characterizing the scaling relationship between subtrochanteric mediolateral diameter and anteroposterior diameter includes 1.0 (0.83—1.04), justifying the treatment of these data as a ratio. The Dinaledi femora are more platymeric than early *Homo*, but less so than that found in *H. erectus* (though this is not significant with the current sample sizes: $p = 0.13$).

Figure 23. Head/neck anteversion of *Homo naledi* compared to fossil hominins and extant humans and chimpanzees. The box-and-whiskers plot shows the median (dark horizontal line), upper and lower quartiles (boxes), range (whiskers), and outliers (circles). *Australopithecus*: A.L. 288-1AP, A.L. 333-95, StW 99, MH1; hominin indet.: KNM-ER 3728; early *Homo*: KNM-ER 1472, KNM-ER 1481; *H. naledi*: U.W. 101-002, U.W. 101-398, U.W. 101-1391, U.W. 101-1475.

They may also be the by-product of a more medial insertion of mm. obturator internus and gemelli, the function of which may therefore be subtly different in *H. naledi* compared with other hominins and with modern humans. The apparent presence of this feature in the immature specimens (i.e., U.W. 101-938) might signify that the anatomy is not the result of bony adaptation, and would therefore lend toward the latter hypothesis. Further research, however, is needed to test these hypotheses.

4.2. Patella

There are very few fossil patellae of early hominins. The earliest is from *A. sediba* (DeSilva et al., 2013). Other patellae are known from the Dmanisi locality (Pontzer et al., 2010, *H. erectus*), Swartkrans (Susman et al., 2001, *A. robustus*), Gran Dolina (Carretero et al., 1999, *Homo antecessor*), Sima de los Huesos (Carretero et al., 1999, *Homo heidelbergensis*), Liang Bua (Jungers et al., 2009, *H. floresiensis*), and a variety of Neanderthal localities (compiled in Carretero et al., 1999). The *H. naledi* knee is represented by four partial patellae (Fig. 12, Table 4). They are strikingly thick anteroposteriorly, making them more human-like than patellae from *A. sediba*, *A. robustus*, and *H. floresiensis* (Fig. 24, Table 4). In absolute thickness (16.2–18.3 mm), the Dinaledi patellae are similar to the AP thick patellae from Dmanisi (~18 mm; Rightmire, pers. comm.) and Gran Dolina (19.0–19.4 mm), and significantly thicker than patellae from Malapa (13.1 mm), Swartkrans (13.3 mm), and Liang Bua (12.2 mm). Additionally, the Dinaledi patellae are relatively thick (AP/ML*100), with values similar to those found in Middle Pleistocene *Homo*. A thicker patella increases the moment arm of m. quadriceps femoris, which may be a derived *Homo* trait (Lovejoy, 2007). Given the role that a thick

patella has in reducing contractile forces of muscles crossing the knee, and therefore reducing joint reaction forces (Silveira et al., 2006), the thick patella of *H. naledi* may have conferred important selective advantages on a hominin walking, or even running (Bramble and Lieberman, 2004), long distances.

4.3. Tibia

The tibia of *H. naledi* is represented by 31 diaphyseal and distal elements (Fig. 13, Table 1), attributed to a minimum of seven mature and two immature individuals (Table 2). *Homo naledi* is characterized by a mediolaterally compressed tibial shaft (Figs. 13 and 15, Table 5), with an oval cross section at midshaft (observable from natural breaks in the bones) and a smooth anterior border. Although modern human tibial diaphyses often possess triangular cross sections, this feature is variable (Hrdlička, 1898) and some modern human (Jungers et al., 2009) and fossil (Trinkaus, 1983; Trinkaus and Ruff, 1999) hominin specimens have oval cross sections.

The proximal attachment for the m. tibialis posterior is large and more posteriorly positioned than is typical in modern humans; the anterior border of the bone is round as in the OH 35 tibia (Susman and Stern, 1982; taxonomic attribution uncertain, but possibly *Homo habilis*; Fig. 15). The platycnemic and midshaft indices of *H. naledi* are in the lower range of variability of modern humans and similar to the average of australopiths and early *Homo* (Table 5). The estimated length of an almost complete tibia (U.W. 101-484) is 325 mm, shorter than that of the immature KNM-WT 15000 (380 mm, Walker and Leakey, 1993, *H. erectus*) and KSD-VP-1/1 (355 mm, Haile-Selassie et al., 2010, *A. afarensis*), but longer than the tibiae of OH 35 (259 mm, Susman and Stern, 1982), A.L. 288-1
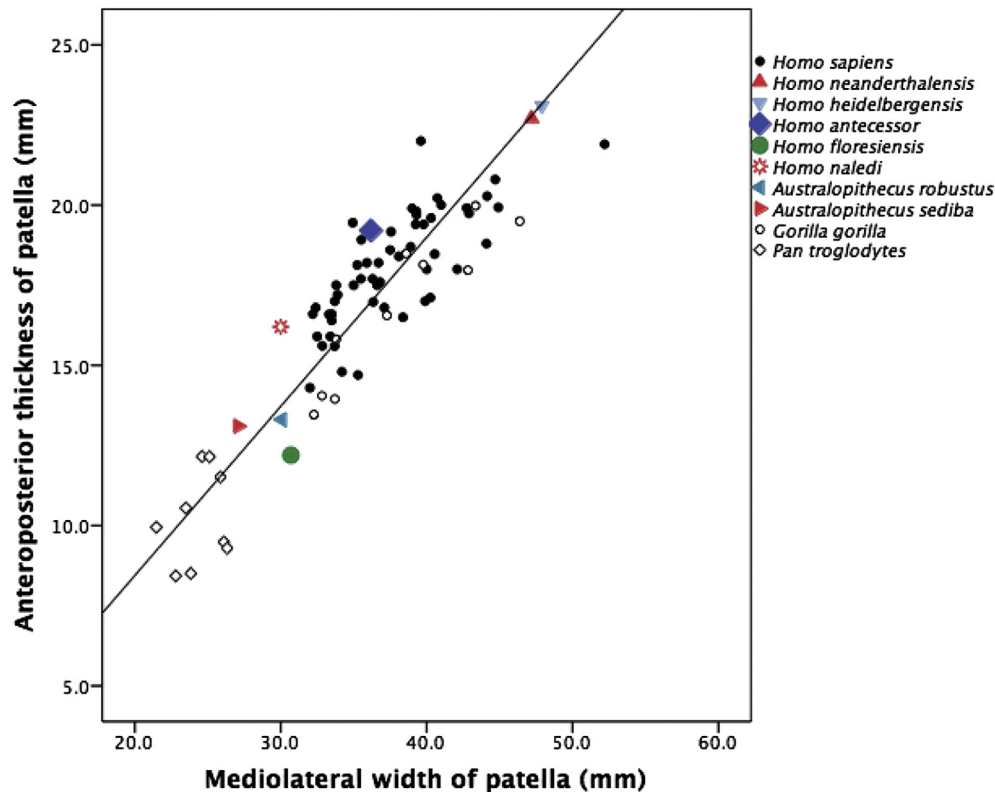
Figure 24. Bivariate plot of mediolateral (ML) diameter by anteroposterior (AP) diameter of the patella of *H. naledi* (star, red in the online version) compared to extant humans (black circles), African apes (gorillas open circles, chimpanzees open diamonds), and other hominins. For the fossil taxa, each symbol represents a single fossil or an average if multiple specimens are known (e.g., Neanderthals). This figure is derived from data in Table 4. A reduced major axis (RMA) regression line is drawn through the extant data: $y = 0.528 \times - 2.11$ ($R^2 = 0.81$). Notice that for a given ML diameter of the patella, humans tend to have AP thicker patellae, while gorillas have AP thinner patellae. The *H. naledi* patella is human-like in its relative thickness.

(227–241 mm, Haile-Selassie et al., 2010; Schmid, 1983, *A. afarensis*), and D3901 (306 mm, Lordkipanidze et al., 2007, *H. erectus*). *Homo naledi* has long tibiae relative to femoral head size, as assessed using a bootstrapping approach (Fig. 25). Compared to the size of the femoral heads in the *H. naledi* assemblage, the nearly complete tibia U.W. 101-484 appears quite long and fits within the human distribution. All other known hominins also fit within the human distribution, though there is overlap between humans and apes (particularly chimpanzees) for this parameter (Fig. 25). Thus, in a similar fashion to early representatives of the genus *Homo* (Pontzer et al., 2010; Holliday, 2012), *H. naledi* possessed relatively long lower limbs, which would have been energetically beneficial during long distance bipedal travel (Pontzer, 2007).

The soleal line of *H. naledi* is well-defined, indicating a strong medial attachment of m. soleus, an important muscle for bipedal locomotion (Myatt et al., 2011). Proximally and medially, *H. naledi* tibiae possess a tubercle for the pes anserinus (SOM Fig. S1), the common insertion of mm. sartorius, gracilis, and semitendinosus. Such a defined insertion—quite distinct from the diffuse rugosity usually detectable in human or fossil hominin tibiae—may indicate an increased role of these muscles in stabilizing the knee of *H. naledi* (Noyes and Sonstegard, 1973). Distally the tibia is similar to other early hominins in possessing an orthogonal orientation of the talar facet relative to the long axis of the shaft (Latimer et al., 1987; DeSilva, 2009). Like other hominins, except *A. sediba*, *H. naledi* has a thin medial malleolus (Fig. 26). There are also long, well-marked insertions for the interosseous and anterior and posterior tibiofibular ligaments and the presence of squatting facets (Fig. 14).

4.4. Fibula

The fibula of *H. naledi* is represented by 42 proximal and diaphyseal elements and two partial distal fibulae (Table 1) attributed to a minimum of eight mature individuals, two immature individuals, and one individual of unknown developmental state (Table 2). The fibular diaphysis of *H. naledi* is gracile relative to its length in comparison to the OH 35 (likely early *Homo*) fibula and to extant chimpanzees (Fig. 18). Estimated length of the most complete bone (U.W. 101-1037), obtained using a regression equation between fibular length and the distance between the neck and the most proximal part of the STS distally, is 328 mm, longer than the OH 35 fibula (estimated at 261.5 mm here and 259 by Susman and Stern, 1982) and in the lower range of modern humans. At the level of the neck, *H. naledi* fibulae are relatively robust (as expressed by ML/AP external diameter) similar to StW 356 (*A. africanus*), MH2 (*A. sediba*), and OH 35, and more robust than modern humans (Table 6). Muscle markings are well-developed along the entirety of the diaphysis, as are the borders that separate the muscle compartments originating from the bone. The attachments of mm. tibialis posterior and peroneus longus are characterized by deep grooves proximally on the medial and lateral surfaces of the fibula, respectively (Fig. 18). The area for the attachment of m. peroneus brevis is convex, as in OH 35 (Davies, 1964; Susman and Stern, 1982) and StW 356, unlike the flat surface seen in modern humans. Distally, a moderately grooved insertion area for the interosseous ligament is present, although the lack of the distal epiphysis on the specimen preserving this area
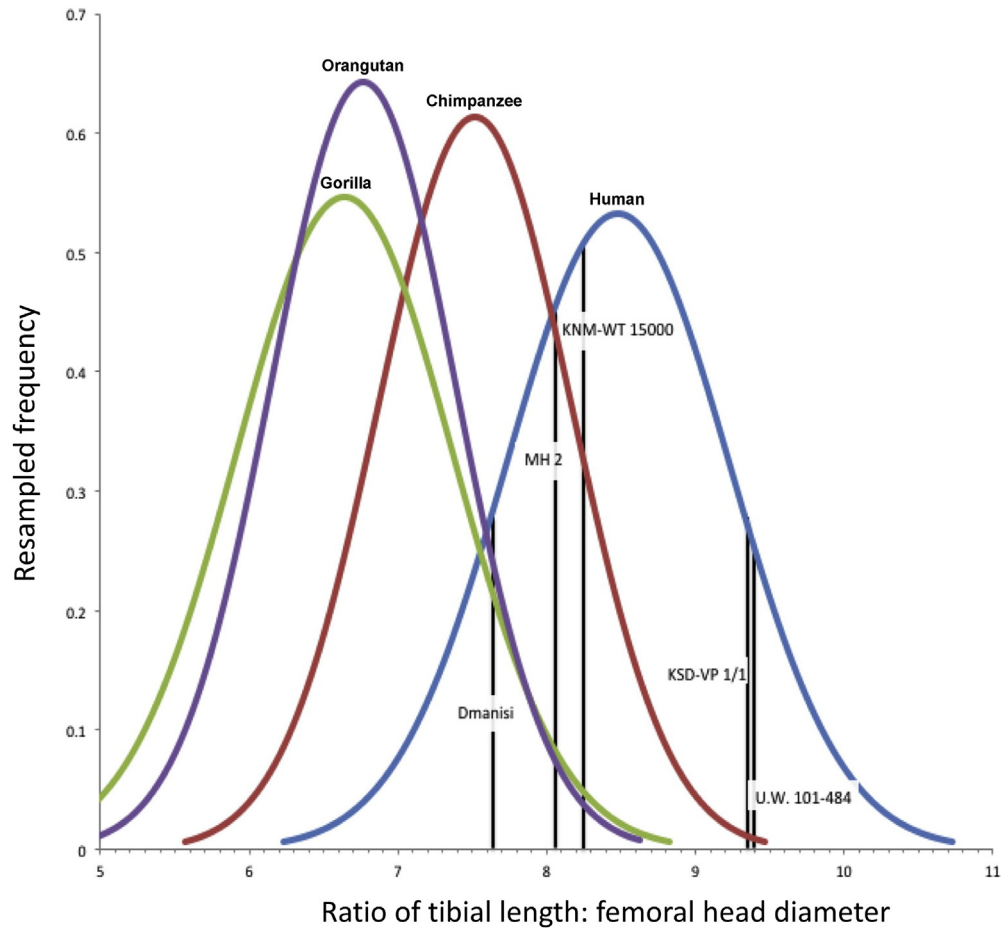
Figure 25. Results of the bootstrap analysis calculating distributions of tibia length: femoral head diameter ratios in orangutans (purple in the online version), gorillas (green in the online version), chimpanzees (red in the online version), and humans (blue in the online version). Fossils are the black vertical lines. Note that extant data and *H. naledi* are derived from bootstrapping analysis of mixed tibial lengths and femoral head diameters, whereas data for the other fossils are based on femoral head diameters and tibial length estimates taken from the same individual (Dmanisi, MH2, KNM-WT 15000, KSD-VP 1/1). The Dinaledi tibia are relatively long compared with the size of the femoral heads currently in the collection.

(U.W. 101-1037) makes it difficult to assess its relative length. The most cranial portion of the subcutaneous triangular surface is at the same level as the most cranial portion of the interosseous ligament insertion, similar to the anatomy in the StW 356 and OH 35 fibulae. In modern humans, the most cranial portions of the two areas are more distant. The distal fibulae of *H. naledi* have a lateral malleolus facing less anteriorly than apes and within the range of modern humans (Table 6).

5. Summary and conclusions

The thigh and leg of *H. naledi* are characterized by a mosaic of primitive traits found in australopiths and shared-derived traits with early *Homo* (Tables 7 and 8). Although the geological age of the assemblage remains unknown, the anatomy is consistent with a Pleistocene transition from *Australopithecus* to early *Homo*. Thus, the Dinaledi assemblage may be a critically important site for characterizing the lower limb of the earliest members of the genus *Homo*. Alternatively, the assemblage may represent yet another "*Homo*-like" variant during what may have been an adaptive radiation of our genus (Jungers et al., 2009; Berger et al., 2010; Ward et al., 2015).

Primitive traits in the *H. naledi* thigh and leg include an australopith-like AP compressed femoral neck, a mediolaterally compressed tibia (Davies, 1964; Susman and Stern, 1982), a large proximal attachment for m. tibialis posterior (Davies, 1964), a relatively circular fibular neck, and a convex surface for the proximal attachment of the m. peroneus brevis on the fibula (Susman and Stern, 1982). Derived traits shared with *Homo* include strong muscle insertions for m. gluteus maximus, well-marked linea aspera, relatively anteroposteriorly thick patellae, a relatively long tibia, and relatively gracile fibulae with laterally oriented lateral malleoli (Davies, 1964; Stern and Susman, 1982; Lovejoy, 2007).

Other features of the lower limb of *H. naledi*, including the presence of two pillars on the superior aspect of the femoral neck (perhaps as a result of a medially extended lateral attachment of the lateral rotators of the hip) and a strong distal attachment of the pes anserinus on the tibia, are unique to the taxon. All of these traits must be considered in the context of a derived foot anatomy (Harcourt-Smith et al., 2015) that suggests that *H. naledi* was a bipedal hominin with adaptations for long distance walking and possibly endurance running (Bramble and Lieberman, 2004; Lieberman et al., 2006; e.g., long legs, enlarged m. gluteus maximus, locking calcaneocuboid joint [Harcourt-Smith et al., 2015]). As with the cranium (Berger et al., 2015), these traits suggest affinity with early *Homo*, including *H. habilis* and *H. erectus*. The largely australopith-like trunk, pelvis, and upper limb (Berger et al., 2015; Kivell et al., 2015) of *H. naledi*, however, demonstrate the mosaic morphology of the species. The significance of this pattern
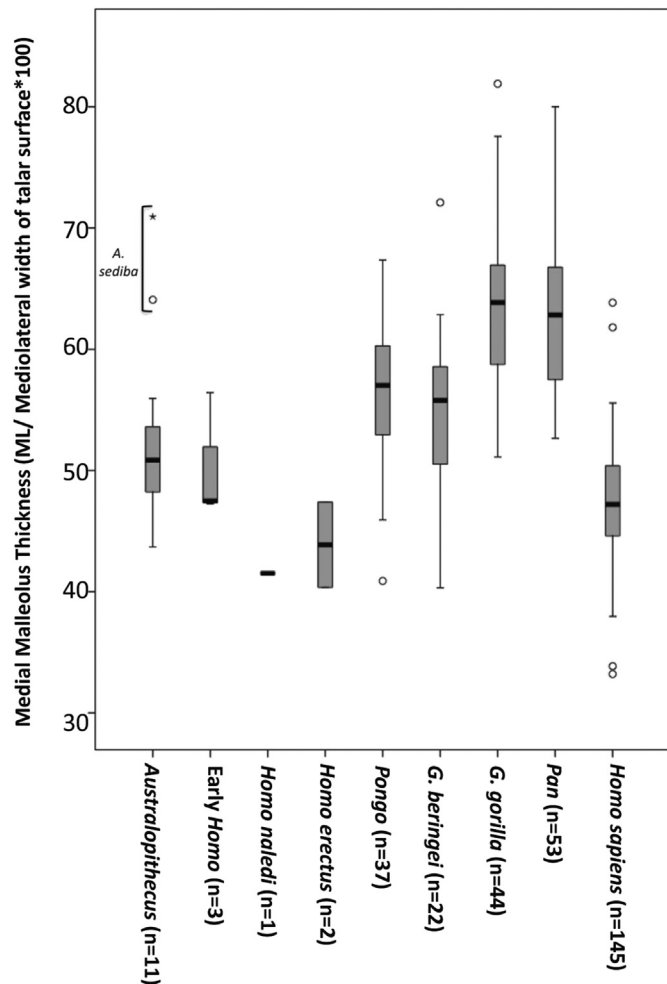
Figure 26. Relative thickness of the medial malleolus of *Homo naledi* compared to fossil hominins and extant humans and apes. The box-and-whiskers plot shows the median (dark horizontal line), upper and lower quartiles (boxes), range (whiskers), and outliers (circles). Individual values are listed in Zipfel et al. (2011).

in the context of hominin evolution, though, is currently unknown, highlighting the importance of further analyses of the unique Dinaledi assemblage.

Supplementary Online Material

Supplementary online material related to this article can be found at http://dx.doi.org/10.1016/j.jhevol.2016.09.005.

References

Aiello, L.C., Dean, C., 2002. An introduction to human evolutionary anatomy. Academic Press, London.

Antón, S.C., Potts, R., Aiello, L.C., 2014. Evolution of early *Homo*: An integrated biological perspective. Science 345, 1236828-1–1236828-13.

Berger, L.R., de Ruiter, D., Churchill, S.E., Schmid, P., Carlson, K.J., Dirks, P.H.G.M., Kibii, J.B., 2010. *Australopithecus sediba*: a new species of *Homo*-like australopith from South Africa. Science 328, 195–204.

Berger, L.E., Hawks, J., de Ruiter, D.J., Churchill, S.E., Schmid, P., Delezene, L., Kivell, T., Garvin, H.M., Williams, S.A., DeSilva, J.M., Skinner, M.M., Musiba, C.M., Cameron, N., Holliday, T.W., Harcourt-Smith, W., Ackermann, R.R., Bastir, M., Bogin, B., Bolter, D., Brophy, J., Cofran, Z.D., Congdon, K.A., Deane, A.S., Dembo, M., Drapeau, M., Elliott, M., Feuerriegel, E.M., Garcia-Martinez, D., Green, D.J., Gurtov, A., Irish, J.D., Kruger, A., Laird, M.F., Marchi, D., Meyer, M.R., Nalla, S., Negash, E.W., Orr, C.M., Radovcic, D., Schroeder, L., Scott, J.E., Throckmorton, Z., Tocheri, M.W., VanSickle, C., Walker, C.S., Wei, P., Zipfel, B., 2015. A new species of the genus *Homo* from the Dinaledi Chamber, South Africa. eLife 4, e09560.

Bramble, D.M., Lieberman, D.E., 2004. Endurance running and the evolution of *Homo*. Nature 432, 345–352.

Carretero, J.M., Lorenzo, C., Arsuaga, J.L., 1999. Axial and appendicular skeleton of *Homo antecessor*. J. Hum. Evol. 37, 459–499.

Chibba, K., Bidmos, M.A., 2007. Using tibia fragments from South Africans of European descent to estimate maximum tibia length and stature. For. Sci. Int. 169, 145–151.

Davies, P.R., 1964. Hominid fossils from Bed I, Olduvai Gorge, Tanganyika. Nature 201, 967–968.

Day, M.H., 1969. Femoral fragment of a robust australopithecine from Olduvai Gorge, Tanzania. Nature 221, 230–233.

Dembo, M., Radovčić, D., Garvin, H.M., Laird, M.F., Schroeder, L., Scott, J., Brophy, J., Ackerman, R.R., Musiba, C.M., de Ruiter, D.J., Mooers, A.Ø., 2016. The evolutionary relationships and age of *Homo naledi*: an assessment using dated Bayesian phylogenetic methods. J. Hum. Evol. 97, 17–26.

DeSilva, J.M., 2008. Vertical climbing adaptations in the anthropoid ankle and midfoot: implications for locomotion in Miocene catarrhines and Plio-Pleistocene hominins. Ph.D. Dissertation, University of Michigan.

DeSilva, J.M., 2009. Functional morphology of the ankle and the likelihood of climbing in early hominins. Proc. Natl. Acad. Sci. 106, 6567–6572.

DeSilva, J.M., Holt, K.G., Churchill, S.E., Carlson, K.J., Walker, C.S., Zipfel, B., Berger, L.R., 2013. The lower limb and mechanics of walking in *Australopithecus sediba*. Science 340, 1232999-1–1232999-5.

Dirks, P.H.G.M., Berger, L.R., Roberts, E.M., Kramers, J., Hawks, J., Randolph-Quinney, P.S., Elliott, M., Musiba, C.M., Churchill, S.E., de Ruiter, D.J., Schmid, P., Backwell, L.R., Belyanin, G.A., Boshoff, P., Hunter, K.L., Feuerriegel, E.M., Gurtov, A., Harrison, J., Hunter, R., Kruger, A., Morris, H., Makhubela, T.V., Peixotto, B., Tucker, S., 2015. Geological and taphonomic context for the new hominin species *Homo naledi* from the Dinaledi Chamber, South Africa. eLife 4, e09561.

Domínguez-Rodrigo, M., Pickering, T.R., Baquedano, E., Mabulla, A., Mark, D.F., Musiba, C., Bunn, H.T., Uribelerrea, D., Smith, V., Diez-Martin, F., Pérez-González, A., 2013. First partial skeleton of a 1.34-million-year-old *Paranthropus boisei* from Bed II, Olduvai Gorge, Tanzania. PLoS One 8, e80347.

Gilbert, W.H., 2008. Daka member hominid postcranial remains. In: Gilbert, W.H., Asfaw, B. (Eds.), *Homo erectus*: Pleistocene evidence from the Middle Awash, Ethiopia, Vol. 1. University of California Press, Cambridge, Berkeley, pp. 373–396.

Haeusler, M., McHenry, H.M., 2004. Body proportions of *Homo habilis* reviewed. J. Hum. Evol. 46, 433–465.

Haeusler, M., McHenry, H.M., 2007. Evolutionary reversals of limb proportions in early hominids? Evidence from KNM-ER 3735 (*Homo habilis*). J. Hum. Evol. 53, 383–405.

Haile-Selassie, Y., Latimer, B.M., Alened, M., Deino, A.L., Gilbert, L., Melillo, S.M., Saylor, B.Z., Scott, G.R., Lovejoy, C.O., 2010. An early *Australopithecus afarensis* postcranium from Woranso-Mille, Ethiopia. Proc. Natl. Acad. Sci. 107, 12121–12126.

Harcourt-Smith, W.E.H., Throckmorton, Z., Congdon, K.A., Zipfel, B., Deane, A.S., Drapeau, M.S.M., Churchill, S.E., Berger, L.R., DeSilva, J.M., 2015. The foot of *Homo naledi*. Nat. Commun. 6, 8432.

Holliday, T.W., 2012. Body size, body shape, and the circumscription of the genus *Homo*. Curr. Anthropol. 53, 330–345.

Hrdlička, A., 1898. Study of the normal tibia. Am. Anthropol. 11 (old series), 307–312.

Jacobs, K., 1992. Estimating femur and tibia length from fragmentary bones: an evaluation of Steele's (1970) method using prehistoric European sample. Am. J. Phys. Anthropol. 89, 333–345.

Johanson, D.C., Masao, F.T., Eck, G.G., White, T.D., Walter, R.C., Kimbel, W.H., Asfaw, B., Manega, P., Ndessokia, P., Suwa, G., 1987. New partial skeleton of *Homo habilis* from Olduvai Gorge, Tanzania. Nature 327, 205–209.

Jungers, W.L., Larson, S.G., Harcourt-Smith, W., Morwood, M.J., Sutikna, T., Awe, R.D., Djubiantono, T., 2009. Descriptions of the lower limb skeleton of *Homo floresiensis*. J. Hum. Evol. 57, 538–554.

Kennedy, G., 1983. Some aspects of femoral morphology in *Homo erectus*. J. Hum. Evol. 12, 587–616.

Kingsley, P.C., Olmsted, K.L., 1948. A study to determine the angle of anteversion of the neck of the femur. J. Bone Joint Surg. 30-A, 745–751.

Kivell, T.L., Deane, A.S., Tocheri, M.W., Orr, C.M., Schmid, P., Hawks, J., Berger, L.R., Churchill, S.E., 2015. The hand of *Homo naledi*. Nat. Commun. 6, 8431.

Latimer, B., Ohman, J.C., Lovejoy, C.O., 1987. Talocrural joint in African hominoids: Implications for *Australopithecus afarensis*. Am. J. Phys. Anthropol. 74, 155–175.

Leakey, M.G., Spoor, F., Dean, M.C., Feibel, C.S., Antón, S.C., Kiarie, C., Leakey, L.N., 2012. New fossils from Koobi Fora in northern Kenya confirm taxonomic diversity in early *Homo*. Nature 488, 201–204.

Leakey, R.E.F., 1973. Evidence from an advanced Plio-Pleistocene hominid from East Rudolf, Kenya. Nature 242, 447–459.

Leakey, R.E.F., Walker, A.C., 1985. Further hominids from the Plio-Pleistocene of Koobi Fora, Kenya. Am. J. Phys. Anthropol. 67, 135–163.

Lieberman, D.E., Raichlen, D.A., Pontzer, H., Bramble, D.M., Cutright-Smith, E., 2006. The human *gluteus maximus* and its role in running. J. Exp. Biol. 209, 2143–2155.

Lordkipanidze, D., Jashashvili, T., Vekua, A., Ponce de León, M., Zollikofer, C.P.E., Rightmire, G.P., Pontzer, H., Ferring, R., Oms, O., Tappen, M., Bukhsianidze, M., Agusti, J., Kahlke, R., Kiladze, G., Martinez-Navarro, B., Mouskhelishvili, A., Nioradze, M., Rook, L., 2007. Postcranial evidence from early *Homo* from Dmanisi, Georgia. Nature 449, 205–310.

Lordkipanidze, D., Ponce de León, M., Margvelashvili, A., Rak, Y., Rightmire, G.P., Vejua, A., Zollikofer, C.P.E., 2013. A complete skull from Dmanisi, Georgia, and the evolutionary biology of Early *Homo*. Science 342, 326–331.

Lovejoy, C.O., 2007. The natural history of human gait and posture. Part 3. The knee. Gait Posture 25, 325–341.

Marchi, D., 2015. Using the morphology of the hominoid distal fibula to interpret arboreality in *Australopithecus afarensis*. J. Hum. Evol. 85, 136–148.

Martin, R., Saller, K., 1957. Lehrbuch der Anthropologie, Vol. I. Fischer Verlag, Stuttgart.

McHenry, H.M., 1994. Early hominid postcrania: phylogeny and function. In: Corruccini, R.S., Chocon, R.L. (Eds.), Integrative paths to the past: Paleoanthropological advances in honor of F. Clark Howell. Prentice Hall, Englewood Cliffs, pp. 251–268.

McHenry, H.M., Corruccini, R.S., 1978. The femur in human evolution. Am. J. Phys. Anthropol. 49, 473–487.

Mosimann, J.E., 1970. Size allometry: size and shape variables with characterizations of the lognormal and generalized Gamma distributions. J. Am. Sta. Assoc. 65, 930–945.

Moyà-Solà, S., Köhler, M., Alba, D., Almécija, S., 2008. Taxonomic attribution of the Olduvai Hominid 7 manual remains and the functional interpretation of hand morphology in the robust australopithecines. Folia Primatol. 79, 215–250.

Myatt, J.P., Schilling, N., Thorpe, S.K.S., 2011. Distribution patterns of fibre types in the triceps surae muscle group of chimpanzees and orangutans. J. Anat. 218, 402–412.

Noyes, F.R., Sonstegard, D.A., 1973. Biomechanical function of the *pes anserinus* at the knee and the effect of its transplantation. J. Bone Joint Surg. Am. 55, 1225–1241.

Ohman, J.C., Krochta, T.J., Lovejoy, C.O., Mensforth, R.P., Latimer, B., 1997. Cortical bone distribution in the femoral neck of hominoids: implications for the locomotion of *Australopithecus afarensis*. Am. J. Phys. Anthropol. 104, 117–131.

Pickford, M., Senut, B., Gommery, D., Treil, J., 2002. Bipedalism in *Orrorin tugenensis* revealed by its femora. CR Palevol. 1, 191–203.

Pontzer, H., 2007. Effective limb length and the scaling of locomotor cost in terrestrial animals. J. Exp. Biol. 210, 1752–1761.

Pontzer, H., Rolian, C., Rightmire, G.P., Jashashvili, T., Ponce de León, M.S., Lordkipanidze, D., Zollikofer, C.P., 2010. Locomotor anatomy and biomechanics of the Dmanisi hominins. J. Hum. Evol. 58, 492–504.

Puymerail, L., Ruff, C.B., Bondioli, L., Widianto, H., Trinkaus, E., Macchiarelli, R., 2012. Structural analysis of the Kresna 11 *Homo erectus* femoral shaft (Sangiran, Java). J. Hum. Evol. 63, 741–749.

Reed, K.E., Kitching, J.W., Grine, F.E., Jungers, W.L., Sokoloff, L., 1993. Proximal femur of *Australopithecus africanus* from Member 4, Makapansgat, South Africa. Am. J. Phys. Anthropol. 92, 1–15.

Richmond, B.R., Jungers, W.L., 2008. *Orrorin tugenensis* femoral morphology and the evolution of hominin bipedalism. Science 319, 1662–1665.

Ruff, C.B., 1995. Biomechanics of the hip and birth in early *Homo*. Am. J. Phys. Anthropol. 98, 527–574.

Ruff, C.B., Higgins, R., 2013. Femoral neck structure and function in early hominins. Am. J. Phys. Anthropol. 150, 512–525.

Schmid, P., 1983. Eine Rekonstruktion des Skelettes von A.L. 288-1 (Hadar) und deren Konsequenzen. Folia Primatol. 40, 283–306.

Silveira, L.F., Bernardes, C., Portella, G., Araujo, F., Loss, J., 2006. Influence of patellar thickness on patellofemoral contact forces and quadriceps muscle forces. J. Biomech. 39, S492.

Sládek, V., Berner, M., Galeta, P., Friedl, L., Kudrnova, S., 2010. Technical Note: The effect of midshaft location on the error ranges of femoral and tibial crosssectional parameters. Am. J. Phys. Anthropol. 141, 325–332.

Spoor, F., Gunz, P., Neubauer, S., Stelzer, S., Scott, N., Kwekason, A., Dean, M.C., 2015. Reconstructed *Homo habilis* type OH 7 suggests deep-rooted species diversity in early *Homo*. Nature 519, 83–86.

Steele, D.G., McKern, T.W., 1969. A method for assessment of maximum long bone length and living stature from fragmentary long bones. Am. J. Phys. Anthropol. 31, 215–228.

Stern, J.T., Susman, R.L., 1983. Locomotor anatomy of *Australopithecus afarensis*. Am. J. Phys. Anthropol. 50, 279–317.

Susman, R.L., Stern, J.T., 1982. Functional morphology of *Homo habilis*. Science 217, 931–934.

Susman, R.L., de Ruiter, D., Brain, C.K., 2001. Recently identified postcranial remains of *Paranthropus* and early *Homo* from Swartkrans Cave, South Africa. J. Hum. Evol. 41, 607–629.

Tardieu, C., 2010. Development of the human hind limb and its importance for the evolution of bipedalism. Evol. Anthropol. 19, 174–186.

Trinkaus, E., 1983. The Shanidar Neandertals. Academic Press, New York.

Trinkaus, E., Ruff, C.B., 1999. Diaphyseal cross-sectional geometry of Near Eastern Middle Paleolithic humans: the tibia. J. Archaeol. Sci. 26, 1289–1300.

Van Arsdale, A., Wolpoff, M.H., 2012. A single lineage in early Pleistocene *Homo*: size variation continuity in early Pleistocene *Homo* crania from East Africa and Georgia. Evolution 67, 841–850.

Van Sickle, C., Williams, S.A., Garcia-Martinez, D., Cofran, Z.D., Churchill, S.E., Berger, L.R., Hawks, J. The pelvis of *Homo naledi*. J. Hum. Evol., in this issue.

Walker, A.C., Leakey, R.E.F., 1993. The postcranial bones. In: Walker, A.C., Leakey, R.E.F. (Eds.), The Nariokotome *Homo erectus* skeleton. Harvard University Press, Cambridge, pp. 95–160.

Ward, C.V., Kimbel, W.H., Harmon, E.H., Johanson, D.C., 2012. New postcranial fossils of Australopithecus afarensis from Hadar, Ethiopia (1990–2007). J. Hum. Evol. 63, 1–51.

Ward, C.V., Feibel, C.S., Hammond, A.S., Leakey, L.N., Moffett, E.A., Plavcan, J.M., Skinner, M.M., Spoor, F., Leakey, M.G., 2015. Associated ilium and femur from Koobi Fora, Kenya, and postcranial diversity in early *Homo*. J. Hum. Evol. 81, 48–67.

Wood, B., Leakey, M., 2011. The Omo-Turkana basin fossil hominins and their contribution to our understanding of human evolution in Africa. Evol. Anthropol. 20, 264–292.

Wright, L.E., Vásquez, M.A., 2003. Estimating the length of incomplete long bones: forensic standards from Guatemala. Am. J. Phys. Anthropol. 120, 223–251.

Zipfel, B., DeSilva, J.M., Kidd, R.S., Carlson, K.J., Churchill, S.E., Berger, L.R., 2011. The foot and ankle of *Australopithecus sediba*. Science 333, 1417–1420.